

# Graph Structure Learning for Spatial-Temporal Imputation: Adapting to Node and Feature Scales

Xinyu Yang<sup>1</sup>, Yu Sun<sup>1\*</sup>, Xinyang Chen<sup>2\*</sup>, Ying Zhang<sup>1</sup>, Xiaojie Yuan<sup>1</sup>

<sup>1</sup>College of Computer Science, DISSec, Nankai University, China

<sup>2</sup>School of Computer Science and Technology, Harbin Institute of Technology, Shenzhen, China  
{yangxinyu@dbis., sunyu@, yingzhang@, yuanxj@}nankai.edu.cn, chenxinyang@hit.edu.cn

## Abstract

Spatial-temporal data collected across different geographic locations often suffer from missing values, posing challenges to data analysis. Existing methods primarily leverage fixed spatial graphs to impute missing values, which implicitly assume that the spatial relationship is roughly the same for all features across different locations. However, they may overlook the different spatial relationships of diverse features recorded by sensors in different locations. To address this, we introduce the multi-scale **Graph Structure Learning** framework for spatial-temporal **Imputation (GSLI)** that dynamically adapts to the heterogeneous spatial correlations. Our framework encompasses node-scale graph structure learning to cater to the distinct global spatial correlations of different features, and feature-scale graph structure learning to unveil common spatial correlation across features within all stations. Integrated with prominence modeling, our framework emphasizes nodes and features with greater significance in the imputation process. Furthermore, GSLI incorporates cross-feature and cross-temporal representation learning to capture spatial-temporal dependencies. Evaluated on six real incomplete spatial-temporal datasets, GSLI showcases the improvement in data imputation.

## Introduction

The stations at different geographic locations may occur missing values when recording spatial-temporal data through multiple kinds of sensors (Zhao et al. 2020b; Fan et al. 2023). Figure 1(a) presents an example of spatial-temporal data with four features recorded by seven stations located in the Netherlands. As shown in Figure 1(b), the readings of feature FH in station AMS at  $t_3$  and feature DD in station DBT at  $t_{17}$  are missing. This may lead to anomalies in the patterns discovered by analysis models, thus creating challenges in mining spatial-temporal data (Ren et al. 2023).

The spatial correlation of spatial-temporal data is usually given as a graph where stations are nodes and edges indicate geographic distance or connectivity between stations (Li et al. 2018; Wu et al. 2019; Fan et al. 2023). Existing works typically utilize the given graph and graph neural networks (GNN) to capture spatial dependencies (Cini,

Marisca, and Alippi 2022; Liu et al. 2023a). Since AMS and DBT stations are geographically closest to each other, their corresponding edge weights in the graph are larger. Therefore, as shown in Figure 1(b), we can get an accurate imputation result of the feature DD in DBT, according to the DD value in AMS station. Unfortunately, this is not always the case, and we can observe that using the FH value in DBT station will mislead the existing methods for imputing the FH value in AMS station. The reason is that features DD and FH are recorded by sensors from different domains, where DD captures wind direction data and FH is related to wind speed. There is a significant correlation between wind direction information from AMS and DBT stations as they are located close to each other. However, since AMS is situated in an airport with a relatively sparse environment and DBT is located in a municipality with many buildings, the relationship between wind speed values of two stations is not clear.

Figure 1(c) illustrates the spatial relationships of different features across all stations, where we extract the attention map from the cross-feature self-attention mechanism. As shown, the spatial relationships for different features are varied, unlike the implicit assumption by existing methods that spatial relationships across stations are similar for different features. In addition, in Figure 1(d), we also find that there is a relatively fixed spatial relationship between the features within each station. Specifically, the attention maps between features within the two stations ELD and ELL are generally similar. This suggests that there also exist correlations between different features across all stations. However, this correlation cannot be reflected in the given graph and thus cannot contribute to the imputation of existing methods.

Enlightened by the aforesaid analysis, we consider the multi-scale **Graph Structure Learning** framework for spatial-temporal **Imputation (GSLI)**. Our main contributions can be summarized as follows.

(1) We present the node-scale graph structure learning to model the fine-grained global spatial correlations of different features. By adaptively learning independent global graph structures for different features, our framework can mitigate the negative effects between features in different domains and improve imputation performance.

(2) We design feature-scale graph structure learning to

\*Corresponding authors.

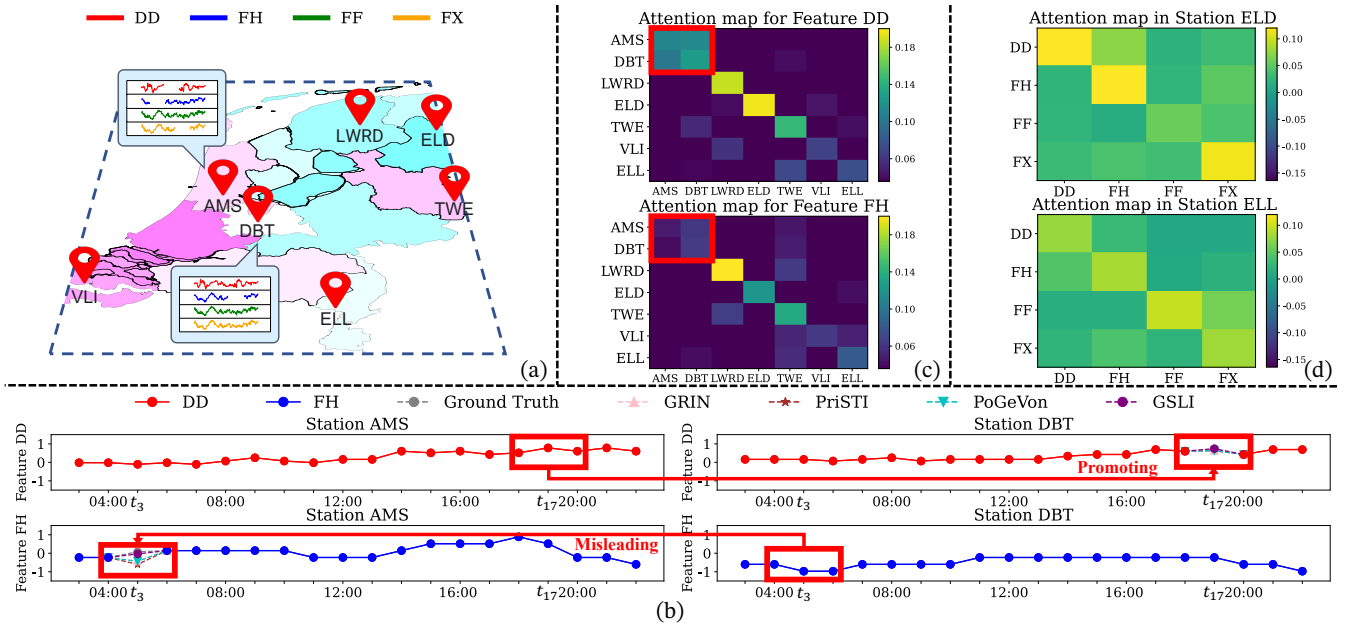


Figure 1: (a) Incomplete spatial-temporal data with four features recorded in different stations in the Netherlands. (b) Imputation examples at timestamps  $t_3$  and  $t_{17}$ . (c) The extracted attention maps for features DD and FH. (d) The extracted attention maps for the four features in stations ELD and ELL.

learn the common spatial correlation of different features over all nodes. Our framework can capture the spatial dependencies between features across each station with the help of the learned feature-scale graph structure.

(3) We incorporate prominence modeling into the graph structure learning processes to account for the varying influence of different nodes and different features. Thus, the nodes and features that contribute more to imputation can get stronger weights in the graph structures.

Experimental evaluations over real-world incomplete datasets demonstrate the superiority of our GSLI, by utilizing cross-feature representation learning and cross-temporal representation learning.

## Related Work

**Spatial-Temporal Imputation** Spatial-temporal data, when viewed as multivariate time series by disregarding spatial correlation, often undergoes imputation using time series imputation methods. Time series imputation utilizes various methods, including statistical approaches like mean imputation (Kantardzic 2011), last observation carried forward (Amiri and Jensen 2016), and local interpolation (Acuna and Rodriguez 2004), alongside techniques such as TRMF (Yu, Rao, and Dhillon 2016), BTMF (Chen and Sun 2022), and TIDER (Liu et al. 2023b) which employ low-rank matrix factorization. RNN-based methods GRU-D (Che et al. 2018) and BRITS (Cao et al. 2018), along with GAN-integrated methods GAN-2-Stage (Luo et al. 2018), E<sup>2</sup>GAN (Luo et al. 2019), SSGAN (Miao et al. 2021b), as well as self-attention and convolutional approaches in STCPA (Xu et al. 2022), SAITS (Du, Côté, and Liu 2023), and TimesNet (Wu et al. 2023) emphasize temporal

dependencies. Moreover, VAEs in MIWAE (Mattei and Frellsen 2019), GP-VAE (Fortuin et al. 2020), TimeCIB (Choi and Lee 2024), diffusion models in CSDI (Tashiro et al. 2021), MIDM (Wang et al. 2023b), SSSD (Alcaraz and Strodthoff 2023), and GPT4TS (Zhou et al. 2023) using large language models are explored. These methods, however, typically ignore the spatial adjacency crucial for spatial-temporal data, indicating potential improvements in the spatial dependency modeling.

For spatial-temporal imputation, LRTC-TNN (Xinyu, Jinming, and Lijun 2020) uses low-rank tensor completion, GRIN (Cini, Marisca, and Alippi 2022) pioneers GNNs, and SPIN (Marisca, Cini, and Alippi 2022) targets error accumulation of GRIN for highly sparse data. STD-GAE (Fan et al. 2023) focuses on denoising graph autoencoders, while DAMR (Ren et al. 2023) dynamically extracts spatial correlations. PriSTI (Liu et al. 2023a) combines diffusion models with GNNs using GWN (Wu et al. 2019), learning rough graph structures. PoGeVon (Wang et al. 2023a) predict missing values over both node time series features and graph structures, ImputeFormer (Nie et al. 2024) and CASPER (Jing et al. 2024) utilize Transformer to capture spatial dependencies. However, these methods often overlook the heterogeneity and common spatial dependencies among different features within nodes (Chen et al. 2023; Chen, Wang, and Xu 2023; Chen et al. 2024). On the contrary, our GSLI addresses feature heterogeneity via node-scale graph structure learning and prominence modeling, while also capturing spatial dependencies between features through feature-scale graph structure learning.

**Spatial-Temporal Graph Structure Learning** In the early stages of modeling spatial-temporal data, researchers commonly use the inherent graph structure and GNN to learn spatial dependencies (Li et al. 2018; Zhao et al. 2020b). Pioneering the enhancement of spatial information within the given graph structure, GWN (Wu et al. 2019) introduces graph structure learning by assigning two learnable embedding vectors to each node. While methods like MTGNN (Wu et al. 2020) and GTS (Shang, Chen, and Bi 2021) design frameworks for learning discrete graph structures, AGCRN (Bai et al. 2020) and CCRNN (Ye et al. 2021) further these advancements by incorporating node-specific convolutions and learning independent graph structures for each convolution layer, respectively. SLCNN (Zhang et al. 2020) aimed to understand both global and local structural information in spatial-temporal data, whereas MegaCRN (Jiang et al. 2023) adapted graph structures based on input signals. CrossGNN (Huang et al. 2023) utilizes graph structure learning to adapt to multiple scales of temporal periods, and heterogeneity between all variables in the forecasting tasks. Unfortunately, these methods often focus on forecasting tasks, ignoring the crucial heterogeneity and correlation between features within nodes and differences in influence between nodes for the imputation task. Compared to the forecasting task, imputing missing values is more difficult to capture temporal dependencies with incomplete observations, thus requiring learning accurate fine-grained spatial dependencies. In contrast, our method captures feature-independent global spatial dependencies and spatial dependencies between features through the node and feature scales of graph structure learning, and reflects differences in node and feature influence by modeling prominence.

## Methodology

In this section, we present the multi-scale Graph Structure Learning framework for spatial-temporal Imputation (GSLI). The framework is built upon node-scale spatial learning, feature-scale spatial learning, cross-feature representation learning, and cross-temporal representation learning.

### Problem Definition

Spatial-temporal data  $\langle \mathcal{G}, \mathbf{X} \rangle$  can be separated into two components: spatial correlation and temporal signal. The spatial correlation is represented by a static graph  $\mathcal{G} = (\mathcal{V}, \mathcal{E})$ , where  $\mathcal{V}$  is the set of  $N$  nodes and  $\mathcal{E}$  is the set of edges reflect the inherent relationships between nodes. The adjacency matrix from  $\mathcal{G}$  is denoted by  $\mathbf{A} \in \mathbb{R}^{N \times N}$ , where  $A_{ij} \in \mathbf{A}$  reflects the weight of the edge  $\langle v_i, v_j \rangle \in \mathcal{E}$ ,  $v_i, v_j \in \mathcal{V}$ . The temporal signal  $\mathbf{X} \in \mathbb{R}^{N \times T \times F}$  is the graph signal obtained by recording  $T$  consecutive timestamps of  $F$  features for each node over  $\mathcal{G}$ . The missing status of  $\mathbf{X}$  can be expressed by the mask matrix  $\mathbf{M} \in \{0, 1\}^{N \times T \times F}$ . If  $m_{i,j,k} \in \mathbf{M}$  is equal to 0, it indicates that the observation  $x_{i,j,k} \in \mathbf{X}$  is missing. Given the incomplete spatial-temporal data, we aim to estimate all missing values  $\mathbf{X} \odot (1 - \mathbf{M})$  in the temporal signal  $\mathbf{X}$ , where  $\odot$  denotes the Hadamard product.

### Node-scale Spatial Learning

To address the challenge of feature heterogeneity, i.e. the objects recorded by the sensors in the station are from different domains, we learn the node-scale graph structure for each feature independently to capture the global spatial dependencies between nodes, as shown in Figure 2. We first split the input representation  $\mathbf{R} \in \mathbb{R}^{N \times T \times F \times C} = \{\mathbf{R}_f \in \mathbb{R}^{N \times T \times C}\}_{f=1}^F$  into  $F$  parts based on features, where  $C$  is the channel number in the deep space for each feature. Then, we adopt the canonical approach (Wu et al. 2019) to assign two learnable meta node embeddings  $\Omega_f^1, \Omega_f^2 \in \mathbb{R}^{N \times d}$  to each feature. We denote  $\Omega_f^1$  as the source node embedding and  $\Omega_f^2$  as the target node embedding. Since the average attention scores for each station obtained through the cross-feature self-attention mechanism are different, it inspires us that different nodes influence the overall imputation differently<sup>1</sup>. To account for the varying influence of different nodes on feature  $f$ , we use the source embedding to learn the prominence vector  $\mathbf{P}_f^\Omega \in \mathbb{R}^{N \times d}$  for each node,

$$\mathbf{P}_f^\Omega = \text{MLP}(\Omega_f^1). \quad (1)$$

To keep the resulting shape not changing, we then utilize the Hadamard product to obtain the refined source embedding  $\hat{\Omega}_f^1$  with  $\mathbf{P}_f^\Omega$ ,

$$\hat{\Omega}_f^1 = \Omega_f^1 \odot \mathbf{P}_f^\Omega. \quad (2)$$

This means that edges sourced from highly influential nodes will carry stronger weight in the learned graph structure. The meta-graph  $\hat{\mathcal{G}}_f^\Omega$  which represents the global spatial correlations specific to the feature  $f$  can be obtained by:

$$\hat{\mathbf{A}}_f^\Omega = \text{SoftMax} \left[ \text{ReLU} \left( \hat{\Omega}_f^1 \Omega_f^2{}^\top \right) \right], \quad (3)$$

where  $\hat{\mathbf{A}}_f^\Omega$  is the adjacency matrix of  $\hat{\mathcal{G}}_f^\Omega$ ,  $\text{ReLU}(\cdot)$  is applied to eliminate the weakly correlated edges of meta-graphs, the  $\text{SoftMax}(\cdot)$  function is used to normalize the adjacency matrices of meta-graphs.

By using the adjacency matrices of both the input graph  $\mathcal{G}$  and the meta-graph  $\hat{\mathcal{G}}_f^\Omega$ , we can use graph diffusion convolution (Li et al. 2018) to capture the node-scale spatial dependencies of signal  $\mathbf{R}_f$ :

$$\mathbf{R}_f^{\text{NL}} = \sum_{k=0}^K \left[ \hat{\mathbf{A}}_f^\Omega \mathbf{R}_f \Theta_{k,f}^{\Omega 1} + \left( \mathbf{D}^{\text{O}-1} \mathbf{A} \right)^k \mathbf{R}_f \Theta_{k,f}^{\Omega 2} + \left( \mathbf{D}^{\text{I}-1} \mathbf{A}^\top \right)^k \mathbf{R}_f \Theta_{k,f}^{\Omega 3} \right], \quad (4)$$

where  $K$  is the step number of the graph diffusion process,  $\Theta_{k,f}^{\Omega 1}, \Theta_{k,f}^{\Omega 2}, \Theta_{k,f}^{\Omega 3} \in \mathbb{R}^{C \times C}$  are graph convolution kernels,  $\mathbf{D}^{\text{O}}$  and  $\mathbf{D}^{\text{I}}$  are the out-degree and in-degree matrices of  $\mathbf{A}$ , respectively. The output  $\mathbf{R}^{\text{NL}} \in \mathbb{R}^{N \times T \times F \times C}$  of node-scale spatial learning is obtained by concatenating the graph diffusion convolution output  $\mathbf{R}_f^{\text{NL}}$  from each feature,

$$\mathbf{R}^{\text{NL}} = \text{Concat}(\mathbf{R}_1^{\text{NL}} \parallel \mathbf{R}_2^{\text{NL}} \dots \parallel \mathbf{R}_F^{\text{NL}}). \quad (5)$$

<sup>1</sup>Please see Prominence Modeling section in Appendix (Yang et al. 2025) for details.

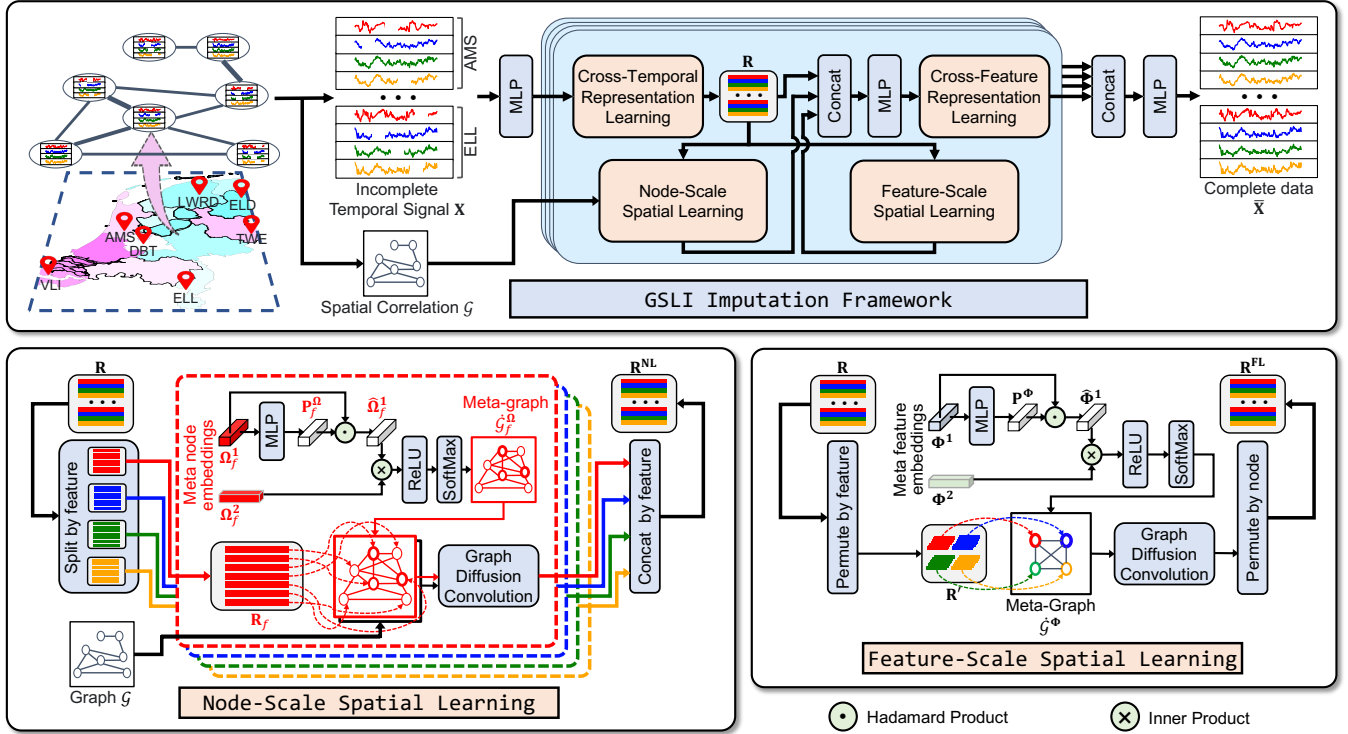


Figure 2: The overview of multi-scale Graph Structure Learning framework for spatial-temporal Imputation (GSLI). GSLI incorporates node-scale spatial learning, which can adapt to feature heterogeneity, and feature-scale spatial learning, which can exploit correlations between features. With cross-feature representation learning and cross-temporal representation learning, GSLI can effectively capture spatio-temporal dependencies for imputation.

This allows us to capture the spatial dependence of each feature independently and avoid the patterns corresponding to different features in this module interfering with each other. For the node-scale spatial learning, the time complexity is  $\mathcal{O}(FN^2TC + FN^2C^2 + FN^2d + FN^2d^2)$ , the space complexity is  $\mathcal{O}(FN^2C + FC^2 + FN^2 + FN^2d + Fd^2)$ . Please refer to the Complexity Analysis section in Appendix (Yang et al. 2025) for a detailed analysis.

If node  $i$  of the graph with feature heterogeneity satisfying the correlation weight of feature  $f_1$  from node  $j$  to node  $i$  is  $x$ , and the correlation weight of feature  $f_2$  from node  $j$  to node  $i$  is  $y \neq x$ , we find the canonical graph convolution cannot address the feature heterogeneity as follows.

**Proposition 1.** *The result of  $\dot{\mathbf{A}}^\Omega \mathbf{R}$  in the first term of the canonical graph diffusion convolution of the channel  $c$  for  $f_2$  feature at timestamp  $t$  for the node  $i$  is*

$$a_{i1}^\Omega r_{1,f_2,c} + \dots + x r_{j,f_2,c} + \dots + a_{iN}^\Omega r_{N,f_2,c},$$

which is in conflict with the expected result  $(a_{i1}^\Omega r_{1,f_2,c} + \dots + y r_{j,f_2,c} + \dots + a_{iN}^\Omega r_{N,f_2,c})$ , where  $\dot{\mathbf{A}}^\Omega \in \mathbb{R}^{N \times N}$  is the learned global graph structure,  $a_{ij}^\Omega \in \dot{\mathbf{A}}^\Omega$ ,  $r_{1,f_2,c}, r_{N,f_2,c}, r_{j,f_2,c} \in \mathbf{R}$ .

Under the same premise, our node-scale spatial learning can also adapt to feature heterogeneity, thus mitigating the misleading of heterogeneous features in neighboring nodes for imputation.

**Proposition 2.** *The result of  $\dot{\mathbf{A}}_f^\Omega \mathbf{R}_f$  in the first term of Equation 4 of the channel  $c$  for  $f_2$  feature at timestamp  $t$  for the node  $i$  is capable to get the expected value:*

$$a_{f_2,i,1}^\Omega r_{f_2,1} + \dots + y r_{f_2,j} + \dots + a_{f_2,i,N}^\Omega r_{f_2,N}.$$

where  $a_{f_2,i,j}^\Omega \in \dot{\mathbf{A}}_{f_2}^\Omega$ ,  $r_{f_2,1}, r_{f_2,N}, r_{f_2,j} \in \mathbf{R}_f$ .

The proofs are based on the information flow analysis, with details in Appendix.Proofs section (Yang et al. 2025).

### Feature-scale Spatial Learning

For modeling the spatial correlation of different features over all nodes, we first define two learnable meta feature embeddings  $\Phi^1, \Phi^2 \in \mathbb{R}^{F \times d}$ , where  $\Phi^1$  is the source feature embedding and  $\Phi^2$  is the target feature embedding. To reflect the influence and heterogeneity of different features, we model the prominence vector  $\mathbf{P}^\Phi \in \mathbb{R}^{F \times d}$  for each feature,

$$\mathbf{P}^\Phi = \text{MLP}(\Phi^1). \quad (6)$$

Next, we refine the source feature embedding  $\Phi^1$  by:

$$\hat{\Phi}^1 = \Phi^1 \odot \mathbf{P}^\Phi. \quad (7)$$

The source feature embeddings for features that are less heterogeneous from other features and can contribute to imputing missing values in other features will have stronger weights. With the inner product between the embeddings,

we can learn the meta-graph  $\hat{\mathcal{G}}^\Phi$  which represents the common spatial correlation of different features within each node,

$$\hat{\mathbf{A}}^\Phi = \text{SoftMax} \left[ \text{ReLU} \left( \hat{\Phi}^1 \Phi^{2^\top} \right) \right], \quad (8)$$

where  $\hat{\mathbf{A}}^\Phi$  denotes the adjacency matrix of  $\hat{\mathcal{G}}^\Phi$ .

To capture the spatial dependencies between different features, we first permute the input  $\mathbf{R} \in \mathbb{R}^{N \times T \times F \times C}$  into  $\mathbf{R}' \in \mathbb{R}^{F \times N \times T \times C}$  according to the features,

$$\mathbf{R}' = \text{Permute}_{(2,0,1,3)}(\mathbf{R}). \quad (9)$$

Then we obtain  $\mathbf{R}'^{\text{FL}}$  through the graph diffusion convolution layer based on  $\hat{\mathcal{G}}^\Phi$ :

$$\mathbf{R}'^{\text{FL}} = \sum_{k=0}^K \hat{\mathbf{A}}^\Phi \mathbf{R}' \Theta_k^\Phi, \quad (10)$$

where  $\Theta_k^\Phi \in \mathbb{R}^{C \times C}$  are graph convolution kernels. The output of the feature-scale spatial learning  $\mathbf{R}^{\text{FL}} \in \mathbb{R}^{N \times T \times F \times C}$  can obtain from permuting the output of the diffusion convolution layer according to the nodes of the input data,

$$\mathbf{R}^{\text{FL}} = \text{Permute}_{(1,2,0,3)}(\mathbf{R}'^{\text{FL}}). \quad (11)$$

### Cross-Feature Representation Learning

The goal of this phase is to self-adaptively obtain the representation that captures spatial dependencies between features across different nodes, which can be challenging to model a large number of spatial dependencies, i.e.,  $(N \times F)^2$ . To overcome this challenge, we use the input representation  $\mathbf{R}$ , with the outputs  $\mathbf{R}^{\text{NL}}$  and  $\mathbf{R}^{\text{FL}}$  obtained from the two scales of spatial learning, as inputs for this stage.

We start by concatenating the three inputs based on features and fusing them using MLP to obtain  $\mathbf{E} \in \mathbb{R}^{N \times T \times F \times C}$ ,

$$\mathbf{E} = \text{MLP} \left[ \text{Concat}(\mathbf{R} \parallel \mathbf{R}^{\text{NL}} \parallel \mathbf{R}^{\text{FL}}) \right]. \quad (12)$$

Then we split  $\mathbf{E} = \{\mathbf{E}_t \in \mathbb{R}^{(N \times F) \times C}\}_{t=1}^T$  into  $T$  segments according to timestamps and merge the node and feature dimensions of each segment. Taking advantage of the Transformer (Vaswani et al. 2017), the learning process to obtain cross-feature representation of each timestamp  $\mathbf{Z}_t \in \mathbb{R}^{(N \times F) \times C}$  is:

$$\mathbf{Z}_t = \text{SoftMax} \left( \frac{\mathbf{Q}_t \mathbf{K}_t^\top}{\sqrt{C}} \right) \mathbf{V}_t, \quad (13)$$

where  $\mathbf{Q}_t = \mathbf{E}_t \mathbf{W}_Q^{\text{CF}}$ ,  $\mathbf{K}_t = \mathbf{E}_t \mathbf{W}_K^{\text{CF}}$ ,  $\mathbf{V}_t = \mathbf{E}_t \mathbf{W}_V^{\text{CF}}$ ,  $\mathbf{W}_Q^{\text{CF}}$ ,  $\mathbf{W}_K^{\text{CF}}$ ,  $\mathbf{W}_V^{\text{CF}} \in \mathbb{R}^{C \times C}$  are learnable parameters. Therefore, we can learn common spatial dependencies across different timestamps. The output cross-feature representation  $\mathbf{Z} \in \mathbb{R}^{N \times T \times F \times C}$  is the result of flattening the node and feature dimensions and concatenating each timestamp,

$$\mathbf{Z} = \text{Concat} \left[ \left\{ \text{Flatten}_{(0,1)}(\mathbf{Z}_t) \right\}_{t=1}^T \right]. \quad (14)$$

The time complexity of this module is  $\mathcal{O}(F^2 NTC + FNTC^2 + F^2 d + Fd^2)$ , the space complexity is  $\mathcal{O}(FNTC + C^2 + F^2 + Fd + d^2)$ . For a detailed analysis, please see the Complexity Analysis section in Appendix (Yang et al. 2025).

### Cross-Temporal Representation Learning

Our goal in this stage is to capture temporal dependencies that can improve the performance of imputation. Since capturing temporal dependencies on the original input signal is more reliable (Zhang, Zheng, and Qi 2017; Lim et al. 2021), we utilize the input temporal signal  $\mathbf{X}^{\text{I}}$  of the spatial-temporal data as the input.

We first project  $\mathbf{X}^{\text{I}}$  into deep space to obtain  $\mathbf{H} \in \mathbb{R}^{N \times T \times F \times C}$ ,

$$\mathbf{H} = \text{MLP}(\mathbf{X}^{\text{I}}). \quad (15)$$

For capturing dependencies between different timestamps, we split  $\mathbf{H} = \{\mathbf{H}_y \in \mathbb{R}^{T \times C}\}_{y=1}^{(N \times K)}$  into  $(N \times K)$  segments according to all features across all nodes. Next, we can obtain the cross-temporal representation of a feature within a node  $\mathbf{R}_y \in \mathbb{R}^{T \times C}$  by

$$\mathbf{R}_y = \text{SoftMax} \left( \frac{\mathbf{Q}_y \mathbf{K}_y^\top}{\sqrt{C}} \right) \mathbf{V}_y, \quad (16)$$

where  $\mathbf{Q}_y = \mathbf{H}_y \mathbf{W}_Q^{\text{CT}}$ ,  $\mathbf{K}_y = \mathbf{H}_y \mathbf{W}_K^{\text{CT}}$ ,  $\mathbf{V}_y = \mathbf{H}_y \mathbf{W}_V^{\text{CT}}$ . To get the cross-feature representation  $\mathbf{R}$ , we need to concatenate all  $\mathbf{R}_y$  and flatten them based on the node to which the features belong,

$$\mathbf{R} = \text{Flatten}_{(0,3)} \left[ \text{Concat}(\{\mathbf{R}_y\}_{y=1}^{N \times F}) \right]. \quad (17)$$

Therefore, we can learn common temporal dependencies across different features.

### The Framework of GSLI

In this section, we introduce the multi-scale Graph Structure Learning framework for spatial-temporal data Imputation (GSLI). The framework mainly consists of multiple layers with the same architecture. Each layer incorporates our proposed node-scale spatial learning, feature-scale spatial learning, cross-feature representation learning, and cross-temporal representation learning. These components work together to capture the spatial-temporal dependencies required for accurate imputation. Following previous studies (Tashiro et al. 2021; Liu et al. 2023a; Nie et al. 2024), we first learn temporal dependencies and then learn spatial dependencies.

When training the framework, it's impossible to know the ground truth of real missing values. Therefore, we randomly selected some observations from  $\mathbf{X}$  as the training label  $\mathbf{X}^{\text{B}} \in \mathbf{X}$ ,  $\mathbf{X}^{\text{B}} \in \mathbb{R}^{N \times T \times F \times C}$ . We use  $\mathbf{M}^{\text{B}}$  to represent the missing status of  $\mathbf{X}^{\text{B}}$  and compose the remaining observations as the input signal  $\mathbf{X}^{\text{I}} = \mathbf{X} \setminus \mathbf{X}^{\text{B}}$  to the framework. Then, we train GSLI by minimizing  $\mathcal{L}$ :

$$\mathcal{L} = \mathbb{E} \left\| (\mathbf{X}^{\text{B}} - \bar{\mathbf{X}}) \odot \mathbf{M}^{\text{B}} \right\|_2^2, \quad (18)$$

where  $\bar{\mathbf{X}}$  is the output of the framework. Note that to encourage the framework to focus on more diverse temporal and spatial dependencies and enhance adaptability and flexibility, we select different  $\mathbf{X}^{\text{B}}$  for each training step.

When imputing incomplete spatial-temporal data, we utilize the original temporal signal as the input signal  $\mathbf{X}^{\text{I}} = \mathbf{X}$ . The final estimated missing value we obtain is  $\bar{\mathbf{X}} \odot (1 - \mathbf{M})$ .

Dataset	#Nodes	#Timestamps	#Features	Missing	Type
DutchWind (Institute 2023)	7	8688	4	0.92%	Wind
BeijingMEO (2018 2018a)	18	8784	5	0.81%	Meteo
LondonAQ (2018 2018b)	13	10897	3	13.81%	Air Quality
CN (Zheng et al. 2014)	140	2203	6	25.3%	Air Quality
Los (Zhao et al. 2020a)	207	2016	1	1.25%	Traffic
LuohuTaxi (Zhao et al. 2020a)	156	2976	1	24.76%	Traffic

Table 1: Dataset summary

## Experiment

In this section, we evaluate the performance of our GSLI in imputation accuracy. The experiments are conducted on a machine equipped with an Intel Xeon Silver 4314 2.40GHz CPU and an NVIDIA GeForce RTX 4090 24GB GPU. The code and datasets are available online (2025)<sup>2</sup>.

### Experimental Setup

**Datasets** In our experiments, we use six spatial-temporal datasets that have real-world missing values. Due to the unavailability of the ground truth of the missing values, we do not include them in the evaluation of imputation accuracy during comparative experiments, as noted in previous studies (Liu et al. 2023a; Ren et al. 2023). The main characteristics of these datasets are summarized in Table 1. For spatial information, since DutchWind, BeijingMEO, and LondonAQ do not explicitly provide adjacency matrices, we build adjacency matrices using the thresholded Gaussian kernel (Shuman et al. 2013) and the station coordinates following previous works (Liu et al. 2023a; Ren et al. 2023).

**Baselines** We compare with four state-of-the-art multivariate time series imputation methods: CSDI (Tashiro et al. 2021), TimesNet (Wu et al. 2023), SAITS (Du, Côté, and Liu 2023) and GPT4TS (Zhou et al. 2023), as well as seven spatial-temporal imputation methods: LRTC-TNN (Xinyu, Jinming, and Lijun 2020), GRIN (Cini, Marisca, and Alippi 2022), STD-GAE (Fan et al. 2023), DAMR (Ren et al. 2023), PriSTI (Liu et al. 2023a), PoGeVon (Wang et al. 2023a), and ImputeFormer (Nie et al. 2024).

### Imputation Comparison

We first conduct experiments with various missing rates and missing mechanisms to evaluate the imputation of GSLI.

Since we can not access the ground truth of the missing values, we randomly remove different percentages of the observations as imputation labels for evaluation through the Missing Completely at Random (MCAR) mechanism (Bohannon et al. 2005). We evaluate the imputation performance using RMSE (Jeffery, Garofalakis, and Franklin 2006) and MAE (Chai and Draxler 2014), as suggested by previous studies (Fan et al. 2023; Liu et al. 2023a). For both metrics, a smaller value indicates a more accurate imputation. We repeat each experiment five times and report the average results in Table 2. We can find that as the missing rate increases, the imputation performance of most methods decreases due to the reduction of information available to

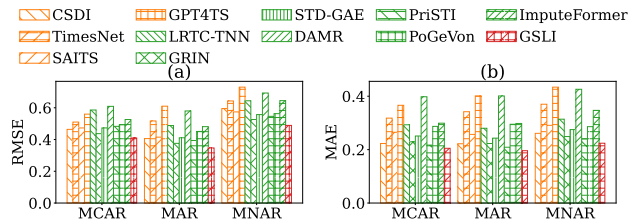


Figure 3: Varying the missing mechanism over DutchWind dataset with 10% missing values

the imputation models. Additionally, we observe that the current spatial-temporal imputation methods do not outperform the multivariate time series imputation methods in a significant manner. This can be attributed to the imprecision of the given graph structure affects the modeling of spatial dependencies. On the contrary, our GSLI achieves consistently superior performance to other methods over different datasets with various missing rates. This is because our GSLI accurately models spatial dependencies through graph structure learning at both the node and feature scales. Moreover, as we learn fine-grained spatial independent correlations for each feature, our method can outperform spatial-temporal imputation methods that only model inter-node dependencies.

Since the occurrence of missing data in real-world scenarios is usually related to the external environment or the sensors themselves, we additionally consider the missing at random (MAR) (Xia et al. 2017) and missing not at random (MNAR) (Twala 2009) mechanisms. Following existing works (Yoon, Jordon, and van der Schaar 2018; Miao et al. 2021a), we explore the imputation performance of different methods with various missing mechanisms. Figure 3 and Missing Mechanisms section in Appendix (Yang et al. 2025) illustrate the performance of different imputation methods with 10% missing values. We find that various imputation methods have similar performance levels with different missing mechanisms. As a result, we use MCAR by default in other experiments. In addition, our GSLI method consistently delivers optimal results across different missing mechanisms. This indicates that the GSLI can adapt well to different real-life missing data scenarios.

### Ablation Study

To validate the efficiency of each component of GSLI, we set up the following ablation variants: **(1) TemporalGCN**: This variant utilizes cross-temporal representation learning to capture temporal dependencies, and the graph diffusion convolution to model spatial dependencies based on the existing adjacency matrix between nodes. **(2) TemporalFeattrueRL**: The temporal dependencies are captured using cross-temporal representation learning, and spatial dependencies are captured using cross-feature representation learning. **(3) w/o Cross-temporal**: We do not use cross-temporal representation learning to capture temporal dependencies in this situation. **(4) w/o Cross-feature**: We do not utilize cross-feature representation learning to model spatial dependencies between features across different nodes. **(5) w/o Feature-Split&Scale**: We replace our node-scale

<sup>2</sup><https://github.com/GSLI25/GSLI25/>

Dataset	Missing rate	Metric	CSDI	TimesNet	SAITS	GPT4TS	LRTC-TNN	GRIN	STD-GAE	DAMR	PriSTI	PoGeVon	ImputeFormer	GSLI	
DutchWind	10%	RMSE	0.464	0.510	0.473	0.560	0.586	0.437	0.473	0.609	0.483	0.493	0.526	<b>0.410</b>	
		MAE	0.223	0.318	0.265	0.366	0.293	0.229	0.251	0.398	0.217	0.287	0.299	<b>0.205</b>	
	20%	RMSE	0.490	0.620	0.482	0.669	0.611	0.441	0.490	0.611	0.489	0.472	0.542	<b>0.421</b>	
		MAE	0.241	0.428	0.272	0.468	0.316	0.234	0.266	0.404	0.227	0.256	0.313	<b>0.213</b>	
	30%	RMSE	0.505	0.717	0.498	0.755	0.659	0.450	0.518	0.615	0.507	0.497	0.551	<b>0.436</b>	
		MAE	0.258	0.515	0.285	0.544	0.349	0.240	0.291	0.407	0.242	0.282	0.321	<b>0.223</b>	
	40%	RMSE	0.526	0.787	0.504	0.817	0.705	0.455	0.564	0.621	0.537	0.569	0.565	<b>0.448</b>	
		MAE	0.284	0.578	0.293	0.600	0.392	0.247	0.337	0.411	0.269	0.364	0.330	<b>0.234</b>	
	BeijingMEO	10%	RMSE	0.466	0.476	0.486	0.527	0.619	0.432	0.485	0.723	0.457	0.534	0.516	<b>0.399</b>
			MAE	0.208	0.306	0.290	0.358	0.322	0.242	0.291	0.510	0.213	0.353	0.283	<b>0.203</b>
		20%	RMSE	0.478	0.528	0.494	0.634	0.658	0.438	0.494	0.730	0.472	0.541	0.527	<b>0.407</b>
			MAE	0.217	0.365	0.303	0.483	0.343	0.248	0.297	0.517	0.229	0.347	0.295	<b>0.210</b>
30%		RMSE	0.490	0.599	0.498	0.720	0.693	0.445	0.500	0.713	0.504	0.535	0.541	<b>0.415</b>	
		MAE	0.227	0.440	0.306	0.571	0.365	0.254	0.301	0.503	0.262	0.333	0.307	<b>0.217</b>	
40%		RMSE	0.506	0.674	0.506	0.788	0.734	0.453	0.508	0.716	0.562	0.562	0.541	<b>0.423</b>	
		MAE	0.240	0.514	0.316	0.636	0.390	0.262	0.306	0.509	0.301	0.364	0.311	<b>0.224</b>	
LondonAQ		10%	RMSE	0.298	0.406	0.375	0.481	0.490	0.311	0.597	0.721	0.314	0.375	0.402	<b>0.272</b>
			MAE	0.182	0.264	0.249	0.321	0.310	0.198	0.471	0.493	0.192	0.232	0.262	<b>0.173</b>
		20%	RMSE	0.321	0.539	0.398	0.633	0.532	0.332	0.609	0.744	0.401	0.395	0.412	<b>0.305</b>
			MAE	0.190	0.358	0.259	0.429	0.334	0.204	0.475	0.499	0.206	0.240	0.266	<b>0.188</b>
	30%	RMSE	0.340	0.658	0.413	0.741	0.584	0.351	0.665	0.786	0.502	0.415	0.436	<b>0.320</b>	
		MAE	0.199	0.449	0.265	0.508	0.367	0.213	0.510	0.522	0.234	0.250	0.275	<b>0.191</b>	
	40%	RMSE	0.375	0.747	0.429	0.811	0.642	0.360	0.631	0.782	0.624	0.428	0.433	<b>0.335</b>	
		MAE	0.210	0.520	0.278	0.564	0.405	0.223	0.495	0.522	0.280	0.263	0.279	<b>0.205</b>	
	CN	10%	RMSE	0.472	0.668	0.474	0.490	0.561	0.403	0.370	0.879	0.387	0.634	0.389	<b>0.253</b>
			MAE	0.182	0.458	0.285	0.315	0.357	0.241	0.205	0.612	0.179	0.394	0.204	<b>0.120</b>
		20%	RMSE	0.436	0.698	0.481	0.509	0.596	0.417	0.388	0.884	0.423	0.633	0.401	<b>0.267</b>
			MAE	0.194	0.485	0.289	0.333	0.387	0.251	0.216	0.622	0.197	0.394	0.210	<b>0.129</b>
30%		RMSE	0.442	0.733	0.490	0.544	0.644	0.434	0.405	0.906	0.477	0.632	0.418	<b>0.282</b>	
		MAE	0.211	0.515	0.297	0.365	0.426	0.264	0.228	0.629	0.226	0.399	0.223	<b>0.139</b>	
40%		RMSE	0.465	0.766	0.499	0.593	0.706	0.451	0.425	0.905	0.512	0.582	0.444	<b>0.299</b>	
		MAE	0.233	0.545	0.304	0.409	0.471	0.277	0.243	0.629	0.262	0.349	0.237	<b>0.150</b>	
Los		10%	RMSE	0.311	0.531	0.535	0.397	0.501	0.295	0.945	0.513	0.293	0.365	0.445	<b>0.263</b>
			MAE	0.177	0.339	0.292	0.257	0.332	0.188	0.541	0.363	0.186	0.209	0.227	<b>0.159</b>
		20%	RMSE	0.333	0.560	0.538	0.452	0.557	0.306	0.942	0.515	0.313	0.377	0.442	<b>0.273</b>
			MAE	0.185	0.365	0.296	0.297	0.372	0.194	0.539	0.362	0.200	0.216	0.223	<b>0.164</b>
	30%	RMSE	0.355	0.602	0.544	0.543	0.618	0.319	0.944	0.521	0.353	0.390	0.459	<b>0.282</b>	
		MAE	0.193	0.401	0.299	0.356	0.415	0.201	0.541	0.368	0.225	0.223	0.230	<b>0.168</b>	
	40%	RMSE	0.398	0.649	0.558	0.651	0.667	0.332	0.944	0.525	0.408	0.401	0.461	<b>0.294</b>	
		MAE	0.210	0.440	0.306	0.422	0.454	0.208	0.541	0.363	0.267	0.230	0.231	<b>0.173</b>	
	LuohuTaxi	10%	RMSE	0.467	0.514	0.452	0.576	0.680	0.436	0.783	0.667	0.523	0.497	0.456	<b>0.410</b>
			MAE	0.313	0.388	0.308	0.429	0.459	0.301	0.612	0.523	0.367	0.340	0.309	<b>0.276</b>
		20%	RMSE	0.468	0.540	0.455	0.692	0.718	0.439	0.780	0.671	0.525	0.498	0.453	<b>0.414</b>
			MAE	0.315	0.415	0.312	0.503	0.489	0.304	0.612	0.527	0.363	0.342	0.308	<b>0.279</b>
30%		RMSE	0.472	0.577	0.456	0.773	0.767	0.443	0.781	0.684	0.531	0.503	0.456	<b>0.419</b>	
		MAE	0.319	0.450	0.312	0.563	0.530	0.307	0.612	0.538	0.370	0.346	0.311	<b>0.283</b>	
40%		RMSE	0.474	0.621	0.461	0.828	0.780	0.448	0.781	0.684	0.537	0.511	0.456	<b>0.424</b>	
		MAE	0.323	0.488	0.317	0.608	0.548	0.311	0.613	0.539	0.374	0.351	0.311	<b>0.287</b>	

Table 2: Imputation performance of GSLI compared to existing methods with various missing rates

Method	DutchWind		BeijingMEO		LondonAQ		CN	
	RMSE	MAE	RMSE	MAE	RMSE	MAE	RMSE	MAE
TemporalGCN	0.4453	0.2335	0.4175	0.2189	0.3133	0.2023	0.2989	0.1492
TemporalFeatueRL	0.4223	0.2062	0.4111	0.2109	0.2926	0.1856	0.3053	0.1520
w/o Cross-temporal	0.4221	0.2124	0.4308	0.2333	0.3515	0.2302	0.3723	0.2104
w/o Cross-feature	0.4140	0.2070	0.4160	0.2214	0.3079	0.1999	0.2609	0.1255
w/o Feature-Split&Scale	0.4147	0.2103	0.4018	0.2051	0.2825	0.1812	0.3100	0.1443
w/o Prominence	0.4132	0.2076	0.4041	0.2080	0.2809	0.1799	0.2595	0.1240
w/o Node-scale	0.4130	0.2081	0.4015	0.2055	0.2845	0.1844	0.2631	0.1263
w/o Feature-scale	0.4213	0.2057	0.4083	0.2093	0.2966	0.1877	0.2932	0.1460
w/o GSL	0.4218	0.2060	0.4090	0.2095	0.2990	0.1907	0.2962	0.1475
GSLI	<b>0.4101</b>	<b>0.2051</b>	<b>0.3986</b>	<b>0.2034</b>	<b>0.2720</b>	<b>0.1730</b>	<b>0.2534</b>	<b>0.1202</b>

Table 3: Ablation analysis of GSLI with 10% missing values

spatial learning and feature-scale spatial learning with the canonical Graph Diffusion Convolution. **(6) w/o Prominence:** When modeling spatial dependencies, the graph structure learning for both scales does not model the prominence of nodes in meta-graphs. **(7) w/o Node-scale:** We only model the spatial correlation between different features for graph structure learning. **(8) w/o Feature-scale:** We learn different node-scale graph structures for different features, and ignore the spatial correlation between features. **(9) w/o GSL:** We do not perform any graph structure learning. Instead, we use the graph diffusion convolution that takes the given adjacency matrix as input and the cross-feature representation learning to learn the spatial dependencies.

Since these variants involve verifying the role of learning graph structures between different features, we performed ablation experiments on four datasets that recorded multiple features, the results are shown in Table 3. The experimental results indicate that each component of the GSLI plays a crucial role, especially in learning the common spatial correlation between different features within nodes for graph structure learning, and performing cross-temporal representation learning. It is worth noting that TemporalGCN consistently performs less than TemporalFeatureSA. This suggests that the given adjacency matrix between nodes cannot accurately reflect the complex spatial correlations in reality. This also confirms the necessity of adopting different scales for learning graph structures.

## Conclusion

In this work, we design the multi-scale Graph Structure Learning framework for spatial-temporal Imputation (GSLI), addressing the challenges of imputing missing values in spatial-temporal data due to feature heterogeneity and latent common correlation between features among all nodes. By applying node-scale and feature-scale graph structure learning alongside prominence modeling, GSLI improves the imputation accuracy, as demonstrated across six diverse datasets with real missing values.

## Acknowledgements

This work is supported in part by the National Natural Science Foundation of China (62302241, 62372252, 72342017, 62306085, 62272250), the Natural Science Foundation of Tianjin (No. 22JCJQC00150), Shenzhen College Stability Support Plan (GXWD20231130151329002).

## References

- 2018, K. C. 2018a. Release page for the Beijing dataset. <https://www.dropbox.com/s/jjta4addnyjndd8/>.
- 2018, K. C. 2018b. Release page for the London dataset. <https://www.dropbox.com/s/ht3yzyx58orxw179/>.
- Acuna, E.; and Rodriguez, C. 2004. The treatment of missing values and its effect on classifier accuracy. In *IFCS*.
- Alcaraz, J. M. L.; and Strodthoff, N. 2023. Diffusion-based Time Series Imputation and Forecasting with Structured State Space Models. *TMLR*.
- Amiri, M.; and Jensen, R. 2016. Missing data imputation using fuzzy-rough methods. *Neurocomputing*, 205: 152–164.
- Bai, L.; Yao, L.; Li, C.; Wang, X.; and Wang, C. 2020. Adaptive Graph Convolutional Recurrent Network for Traffic Forecasting. In *NeurIPS*.
- Bohannon, P.; Flaster, M.; Fan, W.; and Rastogi, R. 2005. A Cost-Based Model and Effective Heuristic for Repairing Constraints by Value Modification. In *SIGMOD*.
- Cao, W.; Wang, D.; Li, J.; Zhou, H.; Li, L.; and Li, Y. 2018. BRITS: Bidirectional Recurrent Imputation for Time Series. In *NeurIPS*.
- Chai, T.; and Draxler, R. R. 2014. Root mean square error (RMSE) or mean absolute error (MAE)?—Arguments against avoiding RMSE in the literature. *Geoscientific model development*, 7(3): 1247–1250.
- Che, Z.; Purushotham, S.; Cho, K.; Sontag, D. A.; and Liu, Y. 2018. Recurrent Neural Networks for Multivariate Time Series with Missing Values. *Scientific reports*, 8(1): 6085.
- Chen, X.; and Sun, L. 2022. Bayesian Temporal Factorization for Multidimensional Time Series Prediction. *IEEE TPAMI*, 44(9): 4659–4673.
- Chen, Y.; Shi, K.; Wang, X.; and Xu, G. 2023. MTSTI: A Multi-task Learning Framework for Spatiotemporal Imputation. In *ADMA*.
- Chen, Y.; Shi, K.; Wu, Z.; Chen, J.; Wang, X.; McAuley, J. J.; Xu, G.; and Yu, S. 2024. A Temporally Disentangled Contrastive Diffusion Model for Spatiotemporal Imputation. *CoRR*, abs/2402.11558.
- Chen, Y.; Wang, X.; and Xu, G. 2023. GATGPT: A Pre-trained Large Language Model with Graph Attention Network for Spatiotemporal Imputation. *CoRR*, abs/2311.14332.
- Choi, M.; and Lee, C. 2024. Conditional Information Bottleneck Approach for Time Series Imputation. In *ICLR*.
- Cini, A.; Marisca, I.; and Alippi, C. 2022. Filling the Gaps: Multivariate Time Series Imputation by Graph Neural Networks. In *ICLR*.
- Du, W.; Côté, D.; and Liu, Y. 2023. SAITS: Self-attention-based imputation for time series. *ESWA*, 219: 119619.
- Fan, Y.; Yu, X.; Wieser, R.; Meakin, D.; Shaton, A.; Jaubert, J.; Flottemesch, R.; Howell, M.; Braid, J.; Bruckman, L. S.; French, R. H.; and Wu, Y. 2023. Spatio-Temporal Denoising Graph Autoencoders with Data Augmentation for Photovoltaic Data Imputation. In *SIGMOD*.
- Fortuin, V.; Baranchuk, D.; Rätsch, G.; and Mandt, S. 2020. GP-VAE: Deep Probabilistic Time Series Imputation. In *AISTATS*.
- Huang, Q.; Shen, L.; Zhang, R.; Ding, S.; Wang, B.; Zhou, Z.; and Wang, Y. 2023. CrossGNN: Confronting Noisy Multivariate Time Series Via Cross Interaction Refinement. In *NeurIPS*.
- Institute, R. N. M. 2023. Release page for the Dutch dataset. <https://www.knmi.nl/nederland-nu/klimatologie/uurgegevens/>.
- Jeffery, S. R.; Garofalakis, M. N.; and Franklin, M. J. 2006. Adaptive Cleaning for RFID Data Streams. In *VLDB*.
- Jiang, R.; Wang, Z.; Yong, J.; Jeph, P.; Chen, Q.; Kobayashi, Y.; Song, X.; Fukushima, S.; and Suzumura, T. 2023. Spatio-Temporal Meta-Graph Learning for Traffic Forecasting. In *AAAI*.
- Jing, B.; Zhou, D.; Ren, K.; and Yang, C. 2024. CASPER: Causality-Aware Spatiotemporal Graph Neural Networks for Spatiotemporal Time Series Imputation. *CoRR*, abs/2403.11960.
- Kantardzic, M. 2011. *Data mining: concepts, models, methods, and algorithms*. John Wiley & Sons.
- Li, Y.; Yu, R.; Shahabi, C.; and Liu, Y. 2018. Diffusion Convolutional Recurrent Neural Network: Data-Driven Traffic Forecasting. In *ICLR*.
- Lim, B.; Arık, S.; Loeff, N.; and Pfister, T. 2021. Temporal Fusion Transformers for interpretable multi-horizon time series forecasting. *International Journal of Forecasting*, 37(4): 1748–1764.
- Liu, M.; Huang, H.; Feng, H.; Sun, L.; Du, B.; and Fu, Y. 2023a. PriSTI: A Conditional Diffusion Framework for Spatiotemporal Imputation. In *ICDE*.
- Liu, S.; Li, X.; Cong, G.; Chen, Y.; and Jiang, Y. 2023b. Multivariate Time-series Imputation with Disentangled Temporal Representations. In *ICLR*.
- Luo, Y.; Cai, X.; Zhang, Y.; Xu, J.; and Yuan, X. 2018. Multivariate Time Series Imputation with Generative Adversarial Networks. In *NeurIPS*.
- Luo, Y.; Zhang, Y.; Cai, X.; and Yuan, X. 2019. E<sup>2</sup>GAN: End-to-End Generative Adversarial Network for Multivariate Time Series Imputation. In *IJCAI*.
- Marisca, I.; Cini, A.; and Alippi, C. 2022. Learning to Reconstruct Missing Data from Spatiotemporal Graphs with Sparse Observations. In *NeurIPS*.
- Mattei, P.; and Frellsen, J. 2019. MIWAE: Deep Generative Modelling and Imputation of Incomplete Data Sets. In *ICML*.



- Miao, X.; Wu, Y.; Chen, L.; Gao, Y.; Wang, J.; and Yin, J. 2021a. Efficient and Effective Data Imputation with Influence Functions. In *VLDB*.
- Miao, X.; Wu, Y.; Wang, J.; Gao, Y.; Mao, X.; and Yin, J. 2021b. Generative Semi-supervised Learning for Multivariate Time Series Imputation. In *AAAI*.
- Nie, T.; Qin, G.; Ma, W.; Mei, Y.; and Sun, J. 2024. ImputeFormer: Low Rankness-Induced Transformers for Generalizable Spatiotemporal Imputation. In *KDD*.
- Pedregosa, F.; Varoquaux, G.; Gramfort, A.; Michel, V.; Thirion, B.; Grisel, O.; Blondel, M.; Prettenhofer, P.; Weiss, R.; Dubourg, V.; VanderPlas, J.; Passos, A.; Cournapeau, D.; Brucher, M.; Perrot, M.; and Duchesnay, E. 2011. Scikit-learn: Machine Learning in Python. *JMLR*, 12: 2825–2830.
- Ren, X.; Zhao, K.; Riddle, P. J.; Taskova, K.; Pan, Q.; and Li, L. 2023. DAMR: Dynamic Adjacency Matrix Representation Learning for Multivariate Time Series Imputation. In *SIGMOD*.
- Shang, C.; Chen, J.; and Bi, J. 2021. Discrete Graph Structure Learning for Forecasting Multiple Time Series. In *ICLR*.
- Shuman, D. I.; Narang, S. K.; Frossard, P.; Ortega, A.; and Vandergheynst, P. 2013. The Emerging Field of Signal Processing on Graphs: Extending High-Dimensional Data Analysis to Networks and Other Irregular Domains. *IEEE SPMAG*, 30(3): 83–98.
- Tashiro, Y.; Song, J.; Song, Y.; and Ermon, S. 2021. CSDI: Conditional Score-based Diffusion Models for Probabilistic Time Series Imputation. In *NeurIPS*.
- Twala, B. 2009. An Empirical Comparison of Techniques for Handling Incomplete Data Using Decision Trees. *AAI*, 23(5): 373–405.
- Vaswani, A.; Shazeer, N.; Parmar, N.; Uszkoreit, J.; Jones, L.; Gomez, A. N.; Kaiser, L.; and Polosukhin, I. 2017. Attention is All you Need. In *NeurIPS*.
- Wang, D.; Yan, Y.; Qiu, R.; Zhu, Y.; Guan, K.; Margenot, A.; and Tong, H. 2023a. Networked Time Series Imputation via Position-aware Graph Enhanced Variational Autoencoders. In *KDD*.
- Wang, X.; Zhang, H.; Wang, P.; Zhang, Y.; Wang, B.; Zhou, Z.; and Wang, Y. 2023b. An Observed Value Consistent Diffusion Model for Imputing Missing Values in Multivariate Time Series. In *KDD*.
- Wu, H.; Hu, T.; Liu, Y.; Zhou, H.; Wang, J.; and Long, M. 2023. TimesNet: Temporal 2D-Variation Modeling for General Time Series Analysis. In *ICLR*.
- Wu, Z.; Pan, S.; Long, G.; Jiang, J.; Chang, X.; and Zhang, C. 2020. Connecting the Dots: Multivariate Time Series Forecasting with Graph Neural Networks. In *KDD*.
- Wu, Z.; Pan, S.; Long, G.; Jiang, J.; and Zhang, C. 2019. Graph WaveNet for Deep Spatial-Temporal Graph Modeling. In *IJCAI*.
- Xia, J.; Zhang, S.; Cai, G.; Li, L.; Pan, Q.; Yan, J.; and Ning, G. 2017. Adjusted weight voting algorithm for random forests in handling missing values. *PR*, 69: 52–60.
- Xinyu, C.; Jinming, Y.; and Lijun, S. 2020. A nonconvex low-rank tensor completion model for spatiotemporal traffic data imputation. *TRC*, 117: 102673.
- Xu, Q.; Ruan, S.; Long, C.; Yu, L.; and Zhang, C. 2022. Traffic Speed Imputation with Spatio-Temporal Attentions and Cycle-Perceptual Training. In *CIKM*.
- Yang, X.; Sun, Y.; Chen, X.; Zhang, Y.; and Yuan, X. 2025. Our code, data and appendix. <https://github.com/GSLI25/GSLI25/>.
- Ye, J.; Sun, L.; Du, B.; Fu, Y.; and Xiong, H. 2021. Coupled Layer-wise Graph Convolution for Transportation Demand Prediction. In *AAAI*.
- Yoon, J.; Jordon, J.; and van der Schaar, M. 2018. GAIN: Missing Data Imputation using Generative Adversarial Nets. In *ICML*.
- Yu, H.; Rao, N.; and Dhillon, I. S. 2016. Temporal Regularized Matrix Factorization for High-dimensional Time Series Prediction. In *NeurIPS*.
- Zhang, J.; Zheng, Y.; and Qi, D. 2017. Deep Spatio-Temporal Residual Networks for Citywide Crowd Flows Prediction. In *AAAI*, 1655–1661.
- Zhang, Q.; Chang, J.; Meng, G.; Xiang, S.; and Pan, C. 2020. Spatio-Temporal Graph Structure Learning for Traffic Forecasting. In *AAAI*.
- Zhao, L.; Song, Y.; Zhang, C.; Liu, Y.; Wang, P.; Lin, T.; Deng, M.; and Li, H. 2020a. Release page for the Los and LuohuTaxi datasets. <https://github.com/lehaifeng/T-GCN/tree/master/T-GCN/T-GCN-PyTorch/data/>.
- Zhao, L.; Song, Y.; Zhang, C.; Liu, Y.; Wang, P.; Lin, T.; Deng, M.; and Li, H. 2020b. T-GCN: A Temporal Graph Convolutional Network for Traffic Prediction. *IEEE TITS*, 21(9): 3848–3858.
- Zheng, Y.; Yi, X.; Li, M.; Li, R.; Shan, Z.; Chang, E.; and Li, T. 2014. Release page for the CN dataset. <http://research.microsoft.com/apps/pubs/?id=246398/>.
- Zhou, T.; Niu, P.; Wang, X.; Sun, L.; and Jin, R. 2023. One Fits All: Power General Time Series Analysis by Pretrained LM. In *NeurIPS*.

## Appendix

### Notations

Table 4 lists our frequently used notations.

### Prominence Modeling

In this section, we present the intuition for introducing the prominence Modeling in the node-scale and feature-scale graph structures learning process in detail.

We first select 10% observations of the original Dutch-Wind (Institute 2023) dataset as the missing values by MCAR mechanism (Bohannon et al. 2005). Then we use cross-temporal self-attention to capture the temporal dependencies and then use cross-feature self-attention to capture the spatial dependencies, based on the setup of the ‘‘TemporalFeatureRL’’ scenario in the Ablation Study section. After that, we use the above architecture to impute missing values. Furthermore, we extract the attention map obtained from cross-feature self-attention after training. Note that this setup is consistent with the survey addressed in Figure 1(c) and Figure 1(d) in the Introduction section.

According to the attention map from the cross-feature self-attention mechanism, we first compute the average attention scores of different stations of each feature. As shown in Figure 4, the average attention score for different stations is different. This suggests the influence for the overall imputation task is different for different stations in the node-scale meta-graph corresponding to each feature.

Then we compute the average attention scores of different features in a station. According to Figure 5, we can find that the average attention score for different features is different. Therefore, the influence for the overall imputation task should be different in the feature-scale meta-graph structure.

The above observation inspires us to perform prominence modeling for the node-scale graph structure learning and feature-scale graph structure learning, as presented in Equation 1, Equation 2, Equation 6, and Equation 7. The process first obtains the corresponding prominence vector self-adaptively based on the input source embedding. And then apply the prominence vector to the source embedding through the Hadamard product to make it enhanced or weakened.

### Proofs

**Proof of Proposition 1** The canonical graph diffusion convolution treats all features on a node as a uniform node embedding. Thus, its convolution operation can be expressed as:

$$\mathbf{R}^{\text{DC}} = \sum_{k=0}^K \left[ \dot{\mathbf{A}}^{\Omega} \mathbf{R} \Theta_k^{\Omega 1} + \left( \mathbf{D}^{\text{O}^{-1}} \mathbf{A} \right)^k \mathbf{R} \Theta_k^{\Omega 2} + \left( \mathbf{D}^{\text{I}^{-1}} \mathbf{A}^{\top} \right)^k \mathbf{R} \Theta_k^{\Omega 3} \right],$$

where  $\dot{\mathbf{A}}^{\Omega} \in \mathbb{R}^{N \times N}$  is the learned global graph structure,  $\mathbf{R} \in \mathbb{R}^{N \times T \times FC}$  is the input graph signal.  $\Theta_k^{\Omega 1}, \Theta_k^{\Omega 2}, \Theta_k^{\Omega 3} \in \mathbb{R}^{FC \times FC}$  are graph convolution kernels.

Symbol	Description
$\mathbf{X}$	incomplete temporal signal of spatial-temporal data with $N$ nodes, $T$ timestamps and $F$ features
$\mathcal{G}$	spatial graph of spatial-temporal data
$\mathbf{M}$	mask matrix indicating the missing status of temporal signal $\mathbf{X}$
$\mathbf{A}$	adjacency matrix of the graph $\mathcal{G}$
$\mathbf{R}$	output of the cross-temporal representation learning module
$\mathbf{R}^{\text{NL}}$	output of the node-scale spatial learning module
$\mathbf{R}^{\text{FL}}$	output of the feature-scale spatial learning module
$\overline{\mathbf{X}}$	output of GSLI framework
$\Omega_f^1, \Omega_f^2$	meta node embeddings of feature $f$
$\dot{\mathbf{A}}_f^{\Omega}$	adjacency matrix of node-scale meta graph $\dot{\mathcal{G}}_f^{\Omega}$ for feature $f$
$\Phi^1, \Phi^2$	meta feature embeddings across all nodes
$\dot{\mathbf{A}}^{\Phi}$	adjacency matrix of feature-scale meta graph $\dot{\mathcal{G}}^{\Phi}$

Table 4: Notations

Considering the feature heterogeneity, then there exists at least one node  $i$  satisfying the correlation weight of feature  $f_1$  from node  $j$  to node  $i$  is  $x$ , and the correlation weight of feature  $f_2$  from node  $j$  to node  $i$  is  $y$ , where  $x \neq y$ . The expected result  $\mathbf{B}$  obtained by multiplying  $\dot{\mathbf{A}}^{\Omega}$  with  $\mathbf{R}$  in the first term of the first order graph diffusion convolution, the corresponding result  $b_{i,t,f_2,c} \in \mathbf{B}$  of the channel  $c$  for  $f_2$  feature at timestamp  $t$  for the node  $i$  is given by:

$$(a_{i1}^{\Omega} r_{1,f_2,c} + \dots + y r_{j,f_2,c} + \dots + a_{iN}^{\Omega} r_{N,f_2,c}),$$

where  $a_{i1}^{\Omega}, a_{iN}^{\Omega} \in \dot{\mathbf{A}}^{\Omega}$ ,  $r_{1,f_2,c}, r_{N,f_2,c}, r_{j,f_2,c} \in \mathbf{R}$ ,  $y$  is the expected value for  $a_{ij}^{\Omega} \in \dot{\mathbf{A}}^{\Omega}$ .

Since the canonical graph diffusion convolution operation has only one learned graph structure, if we assume that  $\dot{\mathbf{A}}^{\Omega}$  satisfies the global correlation for  $f_1$ , then the actual information flow to form the  $b_{i,t,f_2,c} \in \mathbf{B}$  is:

$$b_{i,t,f_2,c} = a_{i1}^{\Omega} r_{1,f_2,c} + \dots + x r_{j,f_2,c} + \dots + a_{iN}^{\Omega} r_{N,f_2,c},$$

which is in conflict with our expected result. Similarly, if we assume that  $\dot{\mathbf{A}}^{\Omega}$  satisfies the global correlation for  $f_2$ , the information flow to form the  $b_{i,t,f_1,c} \in \mathbf{B}$  will conflict with our expected result. Following the same line, we can show that neither the second nor the third term of the graph diffusion convolution addresses the feature heterogeneity.

**Proof of Proposition 2** Similar to Proposition 1, we assume that there exists at least one node  $i$  satisfying the correlation weight of feature  $f_1$  from node  $j$  to node  $i$  is  $x$ , and the correlation weight of feature  $f_2$  from node  $j$  to node  $i$  is  $y$  for the feature heterogeneity problem, where  $x \neq y$ .

According to Equation 3, we learn independent graph structures for each heterogeneous feature. Thus, we suppose that  $a_{f_1,i,j}^{\Omega} = x$ ,  $a_{f_2,i,j}^{\Omega} = y$ , where  $a_{f_1,i,j}^{\Omega} \in \dot{\mathbf{A}}_{f_1}^{\Omega}$  and  $a_{f_2,i,j}^{\Omega} \in \dot{\mathbf{A}}_{f_2}^{\Omega}$ . If the first term of the first order graph

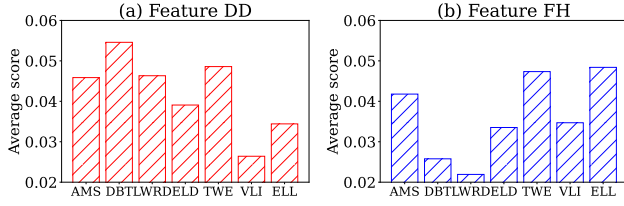


Figure 4: Average attention scores of different stations from cross-feature self-attention mechanism

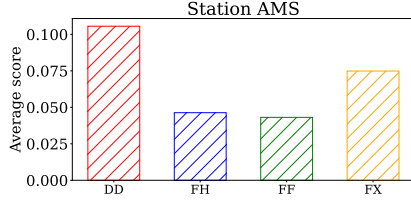


Figure 5: Average attention scores of different features from cross-feature self-attention mechanism

convolution operation shown in Equation 3 operates on the channel  $c$  of feature  $f_2$ , the result obtained by multiplying  $\hat{\mathbf{A}}_{f_2}^\Omega$  with  $\mathbf{R}_{f_2}$  is  $\mathbf{B}_{f_2}$ . The corresponding result of  $\mathbf{B}_{f_2}$  at timestamp  $t$  for the node  $i$  can be obtained by:

$$b_{f_2,i,t} = a_{f_2,i,1}^\Omega r_{f_2,1} + \dots + y r_{f_2,j} + \dots + a_{f_2,i,N}^\Omega r_{f_2,N}.$$

On the other hand, the corresponding result of feature  $f_1$  at timestamp  $t$  for the node  $i$  can be obtained by:

$$b_{f_1,i,t} = a_{f_1,i,1}^\Omega r_{f_1,1} + \dots + x r_{f_1,j} + \dots + a_{f_1,i,N}^\Omega r_{f_1,N}.$$

It can be seen that the heterogeneity of  $f_1$  and  $f_2$  does not affect the correct information flow in our node-scale spatial learning process for the timestamp  $t$ . According to the above process, we can generalize the above result for all heterogeneous feature pairs and all timestamps.

## Complexity Analysis

**Time complexity of Node-scale Spatial Learning** Consider the node-scale spatial learning for feature  $f$ , the complexity to get the prominence vector  $\mathbf{P}_f^\Omega$  is  $\mathcal{O}(Nd^2)$ . Then the complexity to obtain the meta-graph  $\hat{\mathcal{G}}_f^\Omega$  is  $\mathcal{O}(N^2d + Nd^2)$ . For the graph diffusion convolution shown in Equation 4, the complexity of the three convolution terms is both  $\mathcal{O}(N^2TC + NTC^2)$ . Since the graph diffusion convolution step  $K$  is a smaller hyperparameter, the overall time complexity of Equation 4 is  $\mathcal{O}(N^2TC + NTC^2 + N^2d + Nd^2)$ . Finally, Equation 5 concatenates the results obtained on the  $F$  features, so the overall time complexity is  $\mathcal{O}(FN^2TC + FN^2C^2 + FN^2d + FNd^2)$ .

**Space complexity of Node-scale Spatial Learning** For the spatial learning on feature  $f$ , the complexity of Equation 3 is  $\mathcal{O}(Nd + d^2)$ , thus the complexity of obtaining the meta-graph is  $\mathcal{O}(N^2 + Nd + d^2)$ . And the graph diffusion convolution brings a complexity of  $\mathcal{O}(NTC + C^2)$ . Since

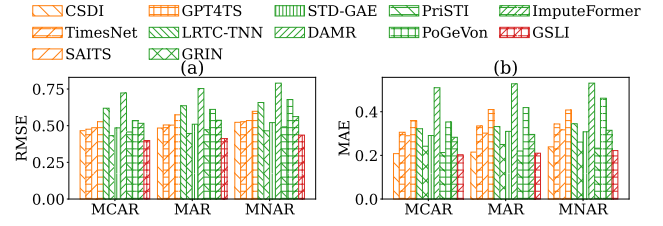


Figure 6: Varying the missing mechanism over BeijingMEO dataset with 10% missing values

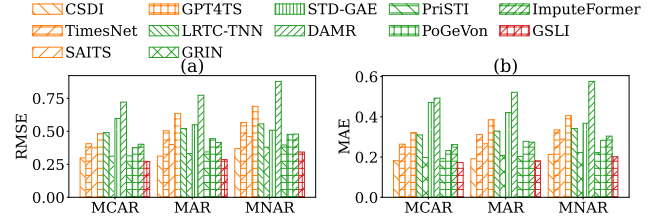


Figure 7: Varying the missing mechanism over LondonAQ dataset with 10% missing values

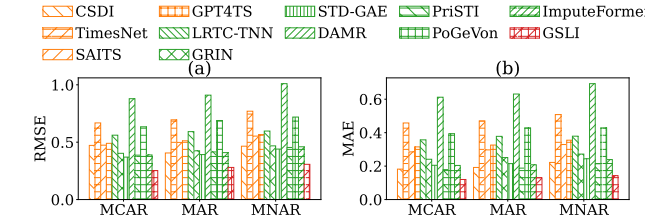


Figure 8: Varying the missing mechanism over CN dataset with 10% missing values

we need to concatenate all the features, the overall space complexity is  $\mathcal{O}(FN^2C + FC^2 + FN^2 + FNd + Fd^2)$ .

## Time complexity of Feature-scale Spatial Learning

First, we need to get the adjacency matrix  $\hat{\mathbf{A}}^\Phi$  of the meta-graph which represents the spatial correlation of different features, the time complexity of this operation is  $\mathcal{O}(F^2d + Fd^2)$ . Then the time complexity of the diffusion convolution layer shown in Equation 10 is  $\mathcal{O}(F^2NTC + FN^2C^2)$ . Therefore, the overall time complexity is  $\mathcal{O}(F^2NTC + FN^2C^2 + F^2d + Fd^2)$ .

## Space complexity of Feature-scale Spatial Learning

Similar to the node-scale spatial learning, the complexity of obtaining the meta-graph  $\hat{\mathcal{G}}^\Phi$  is  $\mathcal{O}(F^2 + Fd + d^2)$ . The space complexity of graph diffusion convolution is  $\mathcal{O}(FN^2C + C^2)$ . The overall space complexity is  $\mathcal{O}(FN^2C + C^2 + F^2 + Fd + d^2)$ .

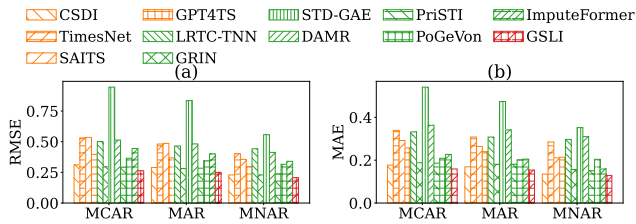


Figure 9: Varying the missing mechanism over Los dataset with 10% missing values

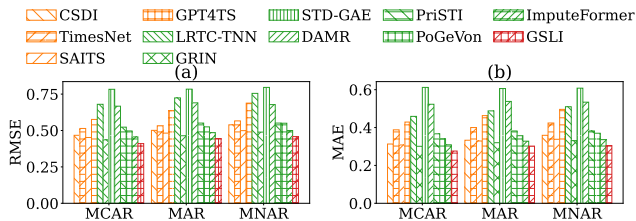


Figure 10: Varying the missing mechanism over LuohuTaxi dataset with 10% missing values

## Supplementary of experiments

**Dataset Details** DutchWind (Institute 2023) gathers wind speed and direction data from 7 stations in the Netherlands hourly from January 1 to December 28, 2023. BeijingMEO (2018 2018a) contains meteorological data recorded at 18 locations in Beijing from January 30, 2017, to January 31, 2018, collected hourly. LondonAQ (2018 2018b) collects hourly air quality readings from January 1, 2017 to March 31, 2018 at 13 locations in London. CN (Zheng et al. 2014) contains hourly air quality data at 140 stations in China from October 1, 2014, to December. 31, 2014. Each station records six features: PM2.5, PM10, NO2, CO, O3, and SO2. Los (Zhao et al. 2020a) contains average traffic speeds per five-minute period from March 1, 2012 to March 7, 2012 at different locations on Los Angeles highways. LuohuTaxi (Zhao et al. 2020a) records the average speed of taxis every 15 minutes on different major roads in Luohu District, Shenzhen in January 2015.

**Missing Mechanisms** In this section, we provide the imputation performance with various missing mechanisms for all datasets.

The occurrence of missing data in real-world scenarios is usually related to the external environment or the sensors themselves. Therefore, we consider three missing mechanisms: missing completely at random (MCAR) (Bohannon et al. 2005), missing at random (MAR) (Xia et al. 2017) and missing not at random (MNAR) (Twala 2009). For MCAR, the missing value is not related to other attributes, and each observation has an equal chance of being missing. MAR potentially implies that the missing status of all features depends on the frequency of a particular feature. For example, missing records of traffic flow data may be related to rush hour and activities in public places. For MNAR, the missing observation depends on the feature itself, for example, the

reliability of recording devices. As in the Imputation Comparison section, we repeat each experiment 5 times for each experiment and report the average results. It should be noted that in all experiments we used different random seeds in our 5 replications, i.e. from 3407 to 3411. Since the random seeds are different, the imputation labels selected in the five replications will also be different.

As shown in Figure 3, Figure 6, Figure 7, Figure 8, Figure 9, and Figure 10, our GSLI method consistently delivers optimal results across different missing mechanisms. It demonstrates that our proposed GSLI is effectively adapted to various missing scenarios in reality. Furthermore, it is important to note that when it comes to the MNAR mechanism, most imputation methods tend to perform slightly worse than the other mechanisms across the majority of datasets. This is because MNAR tends to remove observations in unconventional statuses.

**Mask Strategies of Training Label** For training our GSLI framework, we randomly select some observations as the training label. In this process, the mask ratio and mask pattern to get the training label directly determine the effectiveness of training. Thus, in this section, we explore the performance with different mask ratios and mask patterns.

We first mask different ratios of observations as the training label, the performance of GSLI with different mask ratios is shown in Table 5. We can find that the model performs better when the mask ratio is set to 0.2 or 0.3 in most cases. The training will be easy to converge when the mask ratio is too low, and therefore the model will not be able to accurately learn the required dependencies for imputation. On the contrary, when the mask ratio is too large, it is difficult for the model to mine valid dependencies from training. Therefore, we set the mask ratio to 0.2 by default.

Then we explore the performance when using different mask patterns. Following CSDI (Tashiro et al. 2021) and PriSTI (Liu et al. 2023a), we consider three mask pattern strategies: (1) Block missing (2) Historical missing (3) Random missing. For the ‘‘Historical missing’’ scenario, the mask at the current timestamp has a half probability of being the same as the previous timestamp, and a half probability of performing Random missing. As shown in Table 6, the Block missing or Historical missing strategy is not directly comparable to Random missing in most cases. This is because there is a possibility that the mask pattern may not accurately correspond to the actual missing scenario. Therefore, we default to using the Random missing mask pattern. It should be noted that by comparing the results presented in Table 2, it can be found that benefiting from the learning of multi-scale graph structures, our method consistently outperforms other methods when adjusting the mask strategies in all of them.

Mask Ratio	DutchWind		BeijingMEO		LondonAQ		CN		Los		LuohuTaxi	
	RMSE	MAE	RMSE	MAE	RMSE	MAE	RMSE	MAE	RMSE	MAE	RMSE	MAE
10%	0.4143	0.2080	0.4114	0.2153	0.3034	0.1963	0.2582	0.1233	0.2697	0.1622	0.4186	0.2841
20%	<b>0.4101</b>	0.2051	<b>0.3986</b>	<b>0.2034</b>	0.2720	0.1730	0.2534	<b>0.1202</b>	<b>0.2632</b>	<b>0.1592</b>	<b>0.4102</b>	<b>0.2761</b>
30%	0.4114	<b>0.2038</b>	<b>0.3986</b>	<b>0.2034</b>	0.2718	0.1731	<b>0.2520</b>	0.1203	0.2635	0.1612	0.4147	0.2819
40%	0.4226	0.2124	0.3995	0.2051	<b>0.2708</b>	<b>0.1728</b>	0.2530	0.1207	0.2651	0.1616	0.4174	0.2836
50%	0.4318	0.2179	0.4022	0.2142	0.2800	0.1752	0.2563	0.1227	0.2704	0.1649	0.4183	0.2851

Table 5: Varying the mask ratio of the training label for various datasets with 10% missing values

Mask Pattern	DutchWind		BeijingMEO		LondonAQ		CN		Los		LuohuTaxi	
	RMSE	MAE	RMSE	MAE	RMSE	MAE	RMSE	MAE	RMSE	MAE	RMSE	MAE
Block missing	0.4150	0.2057	0.4089	0.2117	0.3328	0.2197	0.2887	0.1447	0.2759	0.1674	0.4748	0.3209
Historical missing	<b>0.4101</b>	<b>0.2041</b>	0.4013	0.2057	0.3068	0.1989	0.2786	0.1385	0.2636	0.1596	0.4621	0.3080
Random missing	<b>0.4101</b>	0.2051	<b>0.3986</b>	<b>0.2034</b>	<b>0.2720</b>	<b>0.1730</b>	<b>0.2534</b>	<b>0.1202</b>	<b>0.2632</b>	<b>0.1592</b>	<b>0.4102</b>	<b>0.2761</b>

Table 6: Varying the mask pattern of the training label for various datasets with 10% missing values

Methods	Parameters	GPU Memory Usage (MiB)	Time Cost(s)
CSDI	413441	1888	87.78
TimesNet	713692	604	26.25
SAITS	1362896	1044	1.42
GPT4TS	60736540	1386	89.11
LRTC-TNN	-	-	4.96
GRIN	24101	1950	126.01
STD-GAE	3803	432	212.38
DAMR	2977	23080	5518.04
PriSTI	729202	2266	1129.58
PoGeVon	329616	2868	67.09
ImputeFormer	798585	2934	23.70
w/o Feature-Split&Scale	4281781	2354	47.70
GSLI	4478913	2464	47.90

Table 7: Resource consumption over DutchWind dataset with 10% missing values

**Resource Consumption** In this section, we report the resource consumption in Table 7 for our GSLI and existing methods. In this table, we also consider another ablation scenario “w/o FeatureSplit&Feature-scale”. As described in Ablation Study Section, we replace our node-scale Spatial Learning and feature-scale Spatial Learning with the canonical graph diffusion convolution (Li et al. 2018; Wu et al. 2019).

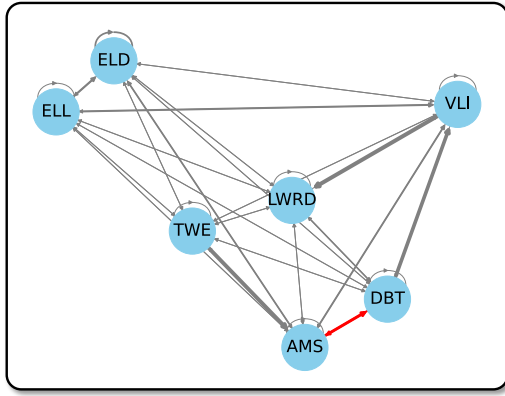
We can find that the overall resource consumption of our method is in the same order of magnitude as the end-to-end deep learning imputation methods. Note that LRTC-TNN is based on low-rank tensor completion with no learnable parameters and no need to utilize GPU training. Since the canonical graph diffusion convolution treats all features on a node as a uniform node embedding, the time complexity is  $\mathcal{O}(FN^2TC + F^N TC^2 + Nd^2)$ , the space complexity is  $\mathcal{O}(FN TC + F^2 C^2)$ . Thus, our resource consumption is slightly higher than the canonical graph diffusion convolution. However, as illustrated in Table 3, our method can produce better imputation results than the above ablation scenario. Therefore, we believe that it is acceptable to pay a small amount of additional resource consumption.

**Graph Structure Visualisation** In this section, we visualize the graph structures we have learned over the DutchWind dataset with 10% missing rate.

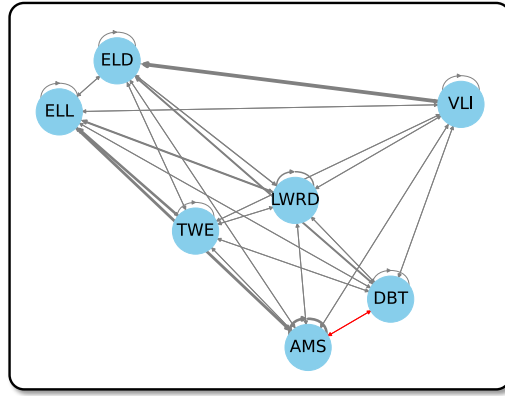
First, we present the learned node-scale meta-graphs for heterogeneous features from our proposed GSLI model, as illustrated in Figure 11. In the presented graphs, thicker edges represent higher edge weights, i.e., more spatial correlations are learned. As mentioned in the Introduction section, feature DD captures wind direction data and FH is related to wind speed. As shown in Figure 1(a), AMS and DBT stations are geographically close to each other. Therefore, there is a stronger spatial correlation between the nodes corresponding to AMS and DBT in the node-scale meta-graph corresponding to the feature DD that records the wind direction. In contrast, due to the large difference in emptiness degrees in the vicinity of AMS and DBT stations, the node-scale meta-graph corresponding to the feature FH for recording wind speeds does not have a strong correlation between the two nodes. This result shows that our GSLI can learn different global node-scale graph structures for features from different domains in response to feature heterogeneity, which also provides an empirical evidence for Proposition 1.

Then we present the learned feature-scale meta-graph, which represents the common spatial correlation of different features over all nodes learned by GSLI. As shown in Figure 12, there is a stronger spatial correlation between FH and FF in the feature-scale meta-graph. Given the strong correlation between features FH and FF, i.e. FH records the hourly average wind speed and FF records the average wind speed in the last 10 minutes of the past hour, it can be shown that GSLI can capture the common spatial correlations of different features over all nodes through the feature-scale graph structure learning.

**Application Study** In this section, we validate different imputation methods for the downstream tasks on the original incomplete LondonAQ dataset. We first impute the missing values through various imputation methods. Then, we eval-



(a) Learned node-scale meta-graph for Feature DD



(b) Learned node-scale meta-graph for Feature FH

Figure 11: Visualisation of the learned node-scale meta-graphs

Method	LondonAQ		LuohuTaxi	
	RMSE	MAE	RMSE	MAE
TimesNet	0.886	0.648	0.372	0.272
GPT4TS	0.885	0.666	0.371	0.266
DCRNN	0.948	0.738	0.764	0.596
GWN	0.967	0.739	0.402	0.300
GTS	0.866	0.665	0.490	0.377
MegaCRN	1.075	0.783	0.373	0.274
CrossGNN	1.052	0.736	0.566	0.423
GSLI	<b>0.806</b>	<b>0.600</b>	<b>0.368</b>	<b>0.267</b>

Table 8: Forecasting performance of GSLI compared to existing methods over real missing datasets

uate the accuracy of air quality forecasts following the same line of existing study (Luo et al. 2019). To be more specific, we use the Adaboost implementation (Pedregosa et al. 2011) to forecast the average PM2.5 concentration at the CD1 station for the next six hours data according to the data from all stations during a 12-hour period. According to Figure 13, most methods with higher imputation accuracies tend to have better air quality forecasting performance. Meanwhile, our method still obtains the best forecasting result, validating its applicability.

**Spatial-Temporal Forecasting** In this section, we directly apply GSLI for downstream spatial-temporal forecasting task on datasets with missing values. We utilize 96 historical timestamps to predict 48 future timestamps for the LondonAQ and LuohuTaxi datasets. To meet the prediction requirements, we introduce an additional linear layer that adjusts the output dimensions to match the forecasting length.

As demonstrated in Table 8, GSLI outperforms existing state-of-the-art methods for spatial-temporal forecasting in situations with missing data. This advantage is due to GSLI’s ability to model complex spatial relationships and adapt its learning of node-scale and feature-scale graph structures to account for feature heterogeneity. In missing scenarios, temporal dependencies are modelled less accurately, but other methods cannot accurately model spatial dependencies, which affects their forecasting performance. The

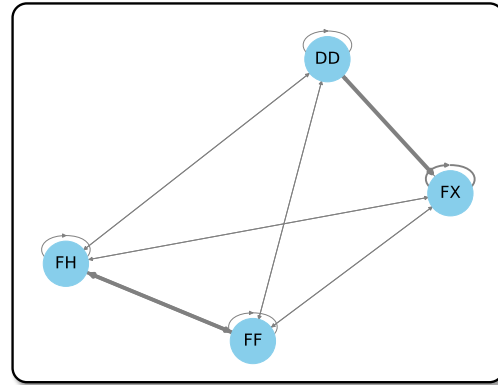


Figure 12: Visualisation of the learned feature-scale meta-graph

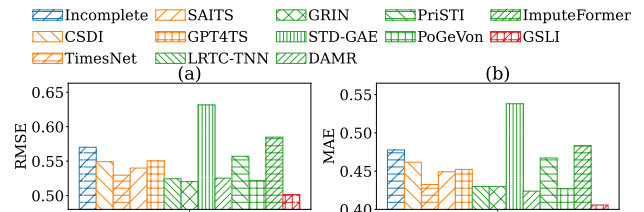


Figure 13: Downstream application results of air quality forecasting over LondonAQ dataset

results confirm GSLI’s superior performance and highlight its robustness in spatial-temporal forecasting when dealing with missing data scenarios.

**Statistical Analysis** In this section, we first conduct a t-test based on the experimental results shown in Table 2. As shown in Table 9, GSLI performs significantly better than various baselines in  $521/528 \approx 98.77\%$  cases under the t-test threshold ( $p < 0.05$ ). Then we report the the average improvement percentage of the imputation performance between existing methods and GSLI based on Table 2, and the results are shown in Table 10. The results show that GSLI shows at least an average improvement of **10.81%** in performance metrics compared to the second-best results.

Dataset	Missing rate	Metric	CSDI	TimesNet	SAITS	GPT4TS	LRTC-TNN	GRIN	STD-GAE	DAMR	PriSTI	PoGeVon	ImputeFormer	GSLI	
DutchWind	10%	RMSE	<b>3.4E-05</b>	<b>4.1E-09</b>	<b>7.4E-07</b>	<b>1.0E-10</b>	<b>2.2E-08</b>	<b>1.6E-04</b>	<b>5.4E-07</b>	<b>4.8E-10</b>	<b>6.6E-07</b>	<b>1.3E-02</b>	<b>2.4E-08</b>	-	
		MAE	<b>4.5E-05</b>	<b>2.2E-12</b>	<b>3.0E-08</b>	<b>2.7E-13</b>	<b>1.2E-10</b>	<b>8.2E-08</b>	<b>3.5E-10</b>	<b>3.7E-10</b>	<b>5.5E-05</b>	<b>3.0E-02</b>	<b>1.0E-10</b>	-	
	20%	RMSE	<b>1.6E-04</b>	<b>3.9E-11</b>	<b>2.1E-05</b>	<b>1.5E-12</b>	<b>3.6E-09</b>	<b>7.4E-04</b>	<b>1.4E-07</b>	<b>1.6E-08</b>	<b>1.1E-07</b>	<b>1.5E-02</b>	<b>3.2E-07</b>	-	
		MAE	<b>3.2E-04</b>	<b>2.7E-14</b>	<b>1.7E-07</b>	<b>8.2E-17</b>	<b>2.7E-11</b>	<b>2.5E-08</b>	<b>6.8E-12</b>	<b>3.8E-10</b>	<b>2.4E-05</b>	<b>1.6E-02</b>	<b>5.8E-09</b>	-	
	30%	RMSE	<b>8.3E-06</b>	<b>1.3E-12</b>	<b>1.2E-06</b>	<b>1.3E-12</b>	<b>5.2E-11</b>	<b>1.2E-02</b>	<b>2.6E-08</b>	<b>1.3E-08</b>	<b>1.9E-06</b>	<b>3.8E-02</b>	<b>1.5E-07</b>	-	
		MAE	<b>1.0E-04</b>	<b>1.4E-15</b>	<b>1.1E-10</b>	<b>1.0E-15</b>	<b>4.6E-11</b>	<b>2.8E-06</b>	<b>3.6E-11</b>	<b>2.4E-11</b>	<b>3.4E-05</b>	<b>4.4E-02</b>	<b>1.3E-09</b>	-	
	40%	RMSE	<b>2.9E-04</b>	<b>5.0E-13</b>	<b>1.8E-06</b>	<b>4.0E-13</b>	<b>2.8E-11</b>	<b>1.5E-01</b>	<b>4.8E-09</b>	<b>3.4E-08</b>	<b>6.5E-05</b>	<b>7.1E-02</b>	<b>3.2E-07</b>	-	
		MAE	<b>8.2E-04</b>	<b>2.8E-14</b>	<b>1.2E-07</b>	<b>1.6E-14</b>	<b>3.7E-11</b>	<b>2.2E-03</b>	<b>3.8E-10</b>	<b>2.2E-10</b>	<b>3.4E-03</b>	<b>6.2E-02</b>	<b>1.5E-08</b>	-	
	BeijingMEO	10%	RMSE	<b>6.5E-08</b>	<b>2.9E-08</b>	<b>8.3E-09</b>	<b>6.6E-10</b>	<b>2.8E-11</b>	<b>1.9E-05</b>	<b>9.3E-09</b>	<b>1.1E-10</b>	<b>6.0E-07</b>	<b>1.0E-07</b>	<b>2.1E-08</b>	-
			MAE	<b>2.2E-01</b>	<b>1.7E-09</b>	<b>1.4E-08</b>	<b>2.2E-10</b>	<b>8.7E-10</b>	<b>6.2E-06</b>	<b>5.4E-09</b>	<b>5.1E-09</b>	<b>4.7E-02</b>	<b>2.7E-07</b>	<b>9.0E-08</b>	-
		20%	RMSE	<b>9.3E-09</b>	<b>2.3E-10</b>	<b>1.8E-09</b>	<b>4.9E-12</b>	<b>8.4E-12</b>	<b>3.8E-06</b>	<b>1.5E-09</b>	<b>3.8E-14</b>	<b>2.1E-07</b>	<b>2.5E-06</b>	<b>9.1E-10</b>	-
			MAE	<b>5.7E-02</b>	<b>3.4E-11</b>	<b>6.0E-09</b>	<b>2.3E-12</b>	<b>1.9E-10</b>	<b>3.4E-06</b>	<b>2.8E-09</b>	<b>1.3E-11</b>	<b>4.5E-03</b>	<b>5.4E-05</b>	<b>2.1E-08</b>	-
30%		RMSE	<b>2.1E-08</b>	<b>2.9E-11</b>	<b>1.4E-08</b>	<b>2.0E-12</b>	<b>2.1E-12</b>	<b>2.4E-05</b>	<b>8.0E-09</b>	<b>3.4E-12</b>	<b>9.3E-06</b>	<b>4.3E-06</b>	<b>1.9E-08</b>	-	
		MAE	<b>2.5E-02</b>	<b>9.3E-12</b>	<b>2.5E-08</b>	<b>9.1E-13</b>	<b>2.3E-10</b>	<b>1.3E-05</b>	<b>1.7E-08</b>	<b>1.3E-10</b>	<b>1.1E-03</b>	<b>5.4E-05</b>	<b>1.0E-07</b>	-	
40%		RMSE	<b>8.8E-09</b>	<b>6.9E-13</b>	<b>4.4E-09</b>	<b>1.9E-13</b>	<b>1.7E-13</b>	<b>1.1E-05</b>	<b>2.8E-09</b>	<b>5.2E-11</b>	<b>5.6E-03</b>	<b>4.3E-04</b>	<b>5.6E-08</b>	-	
		MAE	<b>8.5E-04</b>	<b>2.1E-13</b>	<b>5.3E-09</b>	<b>4.5E-14</b>	<b>1.5E-11</b>	<b>2.0E-06</b>	<b>3.6E-09</b>	<b>8.0E-10</b>	<b>2.5E-04</b>	<b>4.7E-03</b>	<b>5.5E-08</b>	-	
LondonAQ		10%	RMSE	<b>2.0E-03</b>	<b>2.1E-08</b>	<b>1.2E-07</b>	<b>2.0E-09</b>	<b>1.5E-07</b>	<b>1.8E-04</b>	<b>1.2E-11</b>	<b>4.7E-10</b>	<b>3.8E-04</b>	<b>8.8E-07</b>	<b>7.3E-08</b>	-
			MAE	<b>3.1E-02</b>	<b>4.0E-09</b>	<b>4.3E-08</b>	<b>2.6E-10</b>	<b>3.0E-10</b>	<b>8.7E-05</b>	<b>1.2E-12</b>	<b>3.3E-12</b>	<b>1.3E-03</b>	<b>2.3E-07</b>	<b>2.0E-08</b>	-
		20%	RMSE	<b>2.1E-01</b>	<b>4.9E-09</b>	<b>4.0E-05</b>	<b>4.3E-10</b>	<b>1.8E-08</b>	<b>3.3E-02</b>	<b>3.6E-10</b>	<b>4.0E-11</b>	<b>1.1E-02</b>	<b>3.5E-05</b>	<b>9.9E-06</b>	-
			MAE	<b>5.6E-01</b>	<b>4.3E-11</b>	<b>6.5E-07</b>	<b>1.9E-12</b>	<b>1.1E-10</b>	<b>1.2E-03</b>	<b>9.2E-13</b>	<b>1.6E-10</b>	<b>5.7E-03</b>	<b>3.0E-07</b>	<b>1.4E-07</b>	-
	30%	RMSE	<b>2.4E-02</b>	<b>7.6E-12</b>	<b>4.8E-07</b>	<b>2.7E-12</b>	<b>2.3E-11</b>	<b>1.7E-03</b>	<b>3.1E-05</b>	<b>2.5E-10</b>	<b>3.8E-02</b>	<b>3.8E-06</b>	<b>7.7E-07</b>	-	
		MAE	<b>1.2E-01</b>	<b>7.7E-12</b>	<b>1.6E-07</b>	<b>1.5E-12</b>	<b>2.0E-10</b>	<b>1.1E-03</b>	<b>9.1E-07</b>	<b>7.6E-10</b>	<b>7.8E-03</b>	<b>1.9E-06</b>	<b>9.4E-08</b>	-	
	40%	RMSE	<b>8.6E-02</b>	<b>1.5E-12</b>	<b>1.8E-07</b>	<b>6.2E-13</b>	<b>1.1E-10</b>	<b>3.0E-03</b>	<b>8.5E-12</b>	<b>2.7E-09</b>	<b>1.1E-02</b>	<b>1.3E-06</b>	<b>4.6E-07</b>	-	
		MAE	<b>2.2E-01</b>	<b>2.3E-12</b>	<b>4.0E-07</b>	<b>6.6E-13</b>	<b>2.9E-10</b>	<b>3.4E-03</b>	<b>7.8E-12</b>	<b>2.8E-09</b>	<b>5.8E-04</b>	<b>2.4E-06</b>	<b>4.2E-07</b>	-	
	CN	10%	RMSE	<b>5.6E-02</b>	<b>2.2E-13</b>	<b>5.2E-11</b>	<b>2.2E-11</b>	<b>2.6E-12</b>	<b>7.3E-09</b>	<b>4.8E-09</b>	<b>4.9E-14</b>	<b>2.5E-09</b>	<b>4.0E-10</b>	<b>3.3E-09</b>	-
			MAE	<b>2.3E-12</b>	<b>1.8E-16</b>	<b>2.1E-12</b>	<b>2.2E-14</b>	<b>2.3E-17</b>	<b>1.3E-11</b>	<b>8.9E-14</b>	<b>1.0E-15</b>	<b>1.3E-12</b>	<b>3.5E-10</b>	<b>1.9E-10</b>	-
		20%	RMSE	<b>5.7E-03</b>	<b>2.1E-14</b>	<b>4.1E-12</b>	<b>1.3E-13</b>	<b>1.4E-14</b>	<b>3.2E-10</b>	<b>5.8E-11</b>	<b>2.1E-12</b>	<b>5.8E-11</b>	<b>7.3E-09</b>	<b>1.6E-10</b>	-
			MAE	<b>5.2E-13</b>	<b>5.4E-16</b>	<b>2.2E-12</b>	<b>2.8E-15</b>	<b>2.3E-17</b>	<b>2.9E-12</b>	<b>9.3E-14</b>	<b>1.1E-13</b>	<b>9.3E-10</b>	<b>8.6E-08</b>	<b>1.0E-10</b>	-
30%		RMSE	<b>3.1E-05</b>	<b>1.2E-15</b>	<b>1.4E-12</b>	<b>2.7E-14</b>	<b>2.6E-14</b>	<b>1.7E-10</b>	<b>4.4E-12</b>	<b>7.2E-12</b>	<b>2.2E-09</b>	<b>2.3E-06</b>	<b>3.7E-12</b>	-	
		MAE	<b>8.5E-12</b>	<b>2.1E-17</b>	<b>5.9E-12</b>	<b>2.3E-16</b>	<b>2.6E-15</b>	<b>6.5E-12</b>	<b>3.4E-15</b>	<b>1.6E-13</b>	<b>1.1E-08</b>	<b>1.2E-05</b>	<b>2.2E-13</b>	-	
40%		RMSE	<b>7.3E-09</b>	<b>6.6E-17</b>	<b>6.7E-13</b>	<b>1.1E-15</b>	<b>2.3E-13</b>	<b>2.3E-10</b>	<b>1.0E-13</b>	<b>7.5E-13</b>	<b>9.0E-10</b>	<b>7.9E-14</b>	<b>3.2E-12</b>	-	
		MAE	<b>1.4E-10</b>	<b>1.1E-18</b>	<b>1.5E-10</b>	<b>4.6E-16</b>	<b>2.0E-14</b>	<b>1.1E-10</b>	<b>2.0E-15</b>	<b>2.4E-14</b>	<b>4.0E-07</b>	<b>1.3E-13</b>	<b>5.6E-13</b>	-	
Los		10%	RMSE	<b>1.6E-07</b>	<b>2.3E-14</b>	<b>7.3E-13</b>	<b>3.7E-11</b>	<b>2.8E-13</b>	<b>1.4E-06</b>	<b>2.1E-09</b>	<b>3.1E-11</b>	<b>1.0E-05</b>	<b>3.2E-11</b>	<b>5.1E-09</b>	-
			MAE	<b>1.3E-08</b>	<b>1.3E-13</b>	<b>9.5E-14</b>	<b>1.5E-12</b>	<b>4.2E-15</b>	<b>8.7E-07</b>	<b>3.0E-04</b>	<b>1.7E-13</b>	<b>1.6E-07</b>	<b>7.0E-13</b>	<b>4.8E-08</b>	-
		20%	RMSE	<b>7.2E-09</b>	<b>2.2E-14</b>	<b>1.1E-12</b>	<b>2.7E-12</b>	<b>2.1E-15</b>	<b>9.9E-07</b>	<b>2.9E-09</b>	<b>4.3E-11</b>	<b>8.7E-06</b>	<b>8.9E-12</b>	<b>9.3E-13</b>	-
			MAE	<b>1.9E-10</b>	<b>7.5E-15</b>	<b>3.4E-13</b>	<b>1.4E-13</b>	<b>1.9E-17</b>	<b>7.8E-07</b>	<b>3.5E-04</b>	<b>7.7E-12</b>	<b>8.9E-06</b>	<b>1.2E-12</b>	<b>1.0E-10</b>	-
	30%	RMSE	<b>7.9E-10</b>	<b>1.0E-15</b>	<b>9.9E-13</b>	<b>3.3E-10</b>	<b>1.0E-14</b>	<b>1.4E-07</b>	<b>2.8E-09</b>	<b>9.9E-15</b>	<b>4.6E-05</b>	<b>2.0E-12</b>	<b>3.7E-10</b>	-	
		MAE	<b>1.8E-11</b>	<b>1.5E-15</b>	<b>8.2E-14</b>	<b>7.5E-12</b>	<b>1.0E-15</b>	<b>3.6E-07</b>	<b>3.5E-04</b>	<b>7.7E-13</b>	<b>5.1E-05</b>	<b>2.0E-12</b>	<b>2.7E-07</b>	-	
	40%	RMSE	<b>7.7E-05</b>	<b>4.2E-17</b>	<b>1.8E-13</b>	<b>1.7E-10</b>	<b>3.8E-15</b>	<b>3.3E-08</b>	<b>3.1E-09</b>	<b>1.3E-12</b>	<b>1.9E-05</b>	<b>1.8E-10</b>	<b>4.9E-11</b>	-	
		MAE	<b>3.9E-05</b>	<b>3.8E-16</b>	<b>2.9E-12</b>	<b>6.7E-12</b>	<b>1.8E-16</b>	<b>2.5E-08</b>	<b>3.8E-04</b>	<b>2.1E-13</b>	<b>1.2E-05</b>	<b>9.5E-12</b>	<b>7.4E-08</b>	-	
	LuohuTaxi	10%	RMSE	<b>2.0E-09</b>	<b>1.2E-11</b>	<b>1.1E-08</b>	<b>1.7E-08</b>	<b>1.8E-11</b>	<b>8.1E-06</b>	<b>4.7E-04</b>	<b>2.2E-05</b>	<b>4.8E-08</b>	<b>3.4E-09</b>	<b>2.2E-05</b>	-
			MAE	<b>9.7E-10</b>	<b>9.5E-14</b>	<b>2.3E-09</b>	<b>1.6E-09</b>	<b>3.5E-12</b>	<b>1.5E-06</b>	<b>8.4E-05</b>	<b>6.7E-07</b>	<b>2.0E-06</b>	<b>2.3E-10</b>	<b>2.0E-05</b>	-
		20%	RMSE	<b>4.0E-10</b>	<b>1.1E-14</b>	<b>3.7E-11</b>	<b>4.3E-11</b>	<b>6.6E-13</b>	<b>2.1E-08</b>	<b>4.5E-04</b>	<b>1.5E-05</b>	<b>1.0E-10</b>	<b>5.8E-11</b>	<b>1.1E-11</b>	-
			MAE	<b>6.5E-11</b>	<b>3.7E-16</b>	<b>4.5E-10</b>	<b>3.0E-10</b>	<b>3.8E-14</b>	<b>7.6E-08</b>	<b>7.7E-05</b>	<b>3.7E-07</b>	<b>6.4E-08</b>	<b>1.1E-12</b>	<b>4.4E-09</b>	-
30%		RMSE	<b>2.3E-10</b>	<b>1.3E-14</b>	<b>2.0E-09</b>	<b>2.8E-14</b>	<b>3.8E-14</b>	<b>1.8E-08</b>	<b>4.6E-04</b>	<b>3.0E-05</b>	<b>1.0E-11</b>	<b>1.8E-10</b>	<b>2.7E-08</b>	-	
		MAE	<b>1.4E-09</b>	<b>2.7E-16</b>	<b>1.2E-10</b>	<b>2.8E-12</b>	<b>9.9E-16</b>	<b>1.1E-08</b>	<b>7.8E-05</b>	<b>1.3E-06</b>	<b>1.8E-09</b>	<b>1.6E-12</b>	<b>1.6E-08</b>	-	
40%		RMSE	<b>1.4E-10</b>	<b>2.7E-16</b>	<b>2.0E-08</b>	<b>1.1E-14</b>	<b>1.3E-12</b>	<b>4.0E-08</b>	<b>5.1E-04</b>	<b>1.6E-05</b>	<b>4.5E-11</b>	<b>5.7E-12</b>	<b>5.8E-10</b>	-	
		MAE	<b>9.7E-10</b>	<b>7.1E-19</b>	<b>1.0E-09</b>	<b>3.1E-13</b>	<b>9.8E-14</b>	<b>1.1E-08</b>	<b>8.5E-05</b>	<b>1.0E-06</b>	<b>3.7E-10</b>	<b>1.1E-13</b>	<b>2.6E-08</b>	-	

Table 9: T-test P-value (bolding for significant with  $p=0.05$ ) of the imputation performance between GSLI and existing methods with various missing rates

Dataset	Missing rate	Metric	CSDI	TimesNet	SAITS	GPT4TS	LRTC-TNN	GRIN	STD-GAE	DAMR	PriSTI	PoGeVon	ImputeFormer	GSLI
DutchWind	10%	RMSE	11.67%	19.52%	13.38%	26.71%	29.99%	6.20%	13.30%	32.69%	15.03%	16.86%	22.08%	-
		MAE	7.94%	35.56%	22.47%	44.02%	30.06%	10.59%	18.45%	48.51%	5.30%	28.52%	31.51%	-
	20%	RMSE	13.94%	32.05%	12.59%	36.97%	31.05%	4.47%	14.01%	31.02%	13.74%	10.69%	22.23%	-
		MAE	11.53%	50.18%	21.73%	54.51%	32.49%	8.82%	20.01%	47.25%	6.08%	16.68%	31.94%	-
	30%	RMSE	13.71%	39.26%	12.58%	42.26%	33.89%	3.12%	15.83%	29.15%	14.11%	12.33%	20.96%	-
		MAE	13.72%	56.69%	21.78%	59.01%	36.14%	6.94%	23.45%	45.23%	7.84%	20.82%	30.46%	-
40%	RMSE	14.81%	43.05%	11.12%	45.11%	36.37%	1.54%	20.50%	27.76%	16.51%	21.18%	20.58%	-	
	MAE	17.62%	59.48%	20.16%	60.96%	40.26%	5.11%	30.52%	43.02%	12.90%	35.63%	28.97%	-	
BeijingMEO	10%	RMSE	14.49%	16.22%	17.94%	24.38%	35.65%	7.69%	17.88%	44.89%	12.80%	25.30%	22.80%	-
		MAE	2.17%	33.62%	29.85%	43.22%	36.83%	15.80%	30.17%	60.15%	4.52%	42.40%	28.12%	-
	20%	RMSE	14.83%	22.93%	17.59%	35.84%	38.15%	7.17%	17.55%	44.22%	13.83%	24.76%	22.86%	-
		MAE	3.16%	42.39%	30.64%	56.50%	38.75%	15.11%	29.27%	59.35%	8.02%	39.36%	28.68%	-
	30%	RMSE	15.38%	30.83%	16.71%	42.42%	40.20%	6.79%	17.03%	41.82%	17.77%	22.45%	23.33%	-
		MAE	4.57%	50.67%	29.18%	62.00%	40.54%	14.54%	27.98%	56.90%	17.24%	34.83%	29.42%	-
40%	RMSE	16.37%	37.15%	16.26%	46.28%	42.32%	6.58%	16.68%	40.85%	24.66%	24.61%	21.78%	-	
	MAE	6.80%	56.36%	29.16%	64.75%	42.54%	14.60%	26.83%	55.94%	25.46%	38.39%	27.87%	-	
LondonAQ	10%	RMSE	8.83%	32.94%	27.55%	43.45%	44.49%	12.68%	54.46%	62.28%	13.40%	27.55%	32.34%	-
		MAE	5.11%	34.52%	30.52%	46.17%	44.19%	12.49%	63.31%	64.94%	9.86%	25.42%	34.00%	-
	20%	RMSE	4.89%	43.35%	23.42%	51.82%	42.66%	8.14%	49.88%	58.98%	23.91%	22.74%	26.01%	-
		MAE	1.16%	47.59%	27.48%	56.26%	43.80%	7.96%	60.47%	62.38%	8.90%	21.68%	29.33%	-
	30%	RMSE	5.73%	51.36%	22.48%	56.75%	45.20%	8.64%	51.82%	59.28%	36.20%	22.89%	26.50%	-
		MAE	3.73%	57.34%	27.73%	62.28%	47.89%	9.99%	62.44%	63.34%	18.08%	23.42%	30.48%	-
40%	RMSE	10.89%	55.21%	21.92%	58.76%	47.87%	7.06%	47.01%	57.19%	46.35%	21.82%	22.82%	-	
	MAE	3.29%	60.48%	26.07%	63.58%	49.29%	8.07%	58.54%	60.62%	26.76%	21.92%	26.46%	-	
CN	10%	RMSE	46.28%	62.08%	46.60%	48.29%	54.82%	37.08%	31.50%	71.16%	34.53%	60.03%	34.80%	-
		MAE	33.84%	73.76%	57.84%	61.84%	66.36%	50.08%	41.40%	80.37%	32.72%	69.52%	41.07%	-
	20%	RMSE	38.78%	61.75%	44.43%	47.56%	55.14%	35.88%	31.19%	69.77%	36.77%	57.79%	33.31%	-
		MAE	33.81%	73.46%	55.48%	61.30%	66.75%	48.69%	40.42%	79.31%	34.79%	67.34%	38.64%	-
	30%	RMSE	36.15%	61.46%	42.43%	48.11%	56.16%	34.91%	30.23%	68.83%	40.76%	55.30%	32.49%	-
		MAE	34.33%	73.06%	53.33%	61.96%	67.41%	47.35%	39.20%	77.92%	38.64%	65.21%	37.78%	-
40%	RMSE	35.60%	60.91%	39.98%	49.53%	57.61%	33.69%	29.64%	66.92%	41.56%	48.55%	32.52%	-	
	MAE	35.36%	72.39%	50.56%	63.26%	68.08%	45.64%	38.07%	76.07%	42.51%	56.87%	36.43%	-	
Los	10%	RMSE	15.50%	50.45%	50.78%	33.68%	47.47%	10.85%	72.16%	48.72%	10.15%	27.95%	40.81%	-
		MAE	10.20%	53.01%	45.56%	38.04%	51.98%	15.19%	70.56%	56.14%	14.61%	23.86%	29.90%	-
	20%	RMSE	17.94%	51.20%	49.18%	39.56%	50.88%	10.72%	70.98%	46.92%	12.73%	27.42%	38.17%	-
		MAE	11.56%	55.19%	44.77%	44.99%	56.01%	15.60%	69.67%	54.76%	18.34%	24.11%	26.60%	-
	30%	RMSE	20.59%	53.24%	48.28%	48.16%	54.45%	11.70%	70.19%	45.99%	20.17%	27.84%	38.70%	-
		MAE	13.27%	58.19%	43.93%	52.90%	59.63%	16.61%	68.99%	54.44%	25.42%	24.80%	27.07%	-
40%	RMSE	26.19%	54.73%	47.35%	54.91%	55.95%	11.66%	68.89%	44.09%	28.10%	26.86%	36.32%	-	
	MAE	17.51%	60.69%	43.38%	58.99%	61.92%	16.83%	68.00%	52.37%	35.08%	24.85%	25.10%	-	
LuohuTaxi	10%	RMSE	12.19%	20.24%	9.22%	28.82%	39.67%	6.01%	47.59%	38.52%	21.59%	17.40%	10.00%	-
		MAE	11.70%	28.78%	10.46%	35.65%	39.79%	8.28%	54.91%	47.17%	24.70%	18.80%	10.73%	-
	20%	RMSE	11.52%	23.29%	8.89%	40.17%	42.32%	5.70%	46.94%	38.29%	21.17%	16.85%	8.50%	-
		MAE	11.38%	32.70%	10.45%	44.50%	42.91%	8.09%	54.33%	46.96%	22.98%	18.41%	9.33%	-
	30%	RMSE	11.32%	27.38%	8.09%	45.80%	45.35%	5.52%	46.35%	38.77%	21.18%	16.73%	8.22%	-
		MAE	11.38%	37.09%	9.46%	49.74%	46.59%	7.91%	53.79%	47.45%	23.54%	18.21%	9.13%	-
40%	RMSE	10.58%	31.76%	8.00%	48.81%	45.67%	5.31%	45.75%	38.04%	21.02%	17.00%	7.16%	-	
	MAE	11.20%	41.23%	9.62%	52.84%	47.64%	7.75%	53.16%	46.80%	23.20%	18.26%	7.64%	-	

Table 10: Improvement percentage of the imputation performance between existing methods and GSLI with various missing rates